# PP2A-Cdc55 phosphatase coordinates actomyosin ring contraction and septum formation during cytokinesis

Yolanda Moyano-Rodríguez[1], Odena Vilalta-Castany[1], Magdalena Foltman[2,3], Alberto Sanchez-Diaz[2,3] and Ethel Queralt[1,*]

[1]Cell Cycle Group, Institut d'Investigacions Biomèdica de Bellvitge (IDIBELL), Av. Gran Via de L'Hospitalet 199-203, 08908 L'Hospitalet de Llobregat, Barcelona, Spain.

[2]Instituto de Biomedicina y Biotecnología de Cantabria, Universidad de Cantabria, CSIC, Santander, Spain

[3]Departamento de Biología Molecular, Facultad de Medicina, Universidad de Cantabria, Santander, Spain

*Correspondence/lead contact: equeralt@idibell.cat, telephone +34932607128, fax +34932607219. ORCID: 0000-0003-0045-0039

Running head: New PP2A-Cdc55 role in cytokinesis

Keywords: Cell Cycle, cytokinesis, PP2A-Cdc55, ingression progression complexes (IPC), AMR contraction, septum formation

## Summary

Eukaryotic cells divide and separate all their components after chromosome segregation by a process called cytokinesis to complete cell division. Cytokinesis is regulated by exclusive elements of the process, and by some mitotic exit regulators. The mitotic kinases Cdc28-Clb2, Cdc5, and Dbf2-Mob1 phosphorylate cytokinetic proteins in budding yeast, but very little is known about the phosphatases regulating cytokinesis. The PP2A-Cdc55 phosphatase regulates mitosis counteracting Cdk1- and Cdc5-dependent phosphorylations. This prompted us to propose that PP2A-Cdc55 could also regulate cytokinesis by counteracting the mitotic kinases. Here, we demonstrate by in vivo and in vitro assays that PP2A-Cdc55 dephosphorylates the F-BAR protein Hof1 and the chitin synthase Chs2, two components of the Ingression Progression Complexes (IPC) involved in cytokinesis regulation. Primary septum formation and actomyosin ring contraction are impaired in absence of PP2A-Cdc55. Interestingly, the non-phosphorylable version of Chs2 rescue the asymmetric AMR contraction observed in absence of Cdc55, indicating that timely dephosphorylation of the IPC proteins by PP2A-Cdc55 is crucial for proper actomyosin ring contraction and septum formation. These findings reveal a new mechanism of cytokinesis regulation by the PP2A-Cdc55 phosphatase and extend our knowledge in the involvement of multiple phosphatases during cytokinesis.

## Introduction

Cytokinesis is the final event of the cell cycle and mediates the physical separation of mother and daughter cells. It is a highly ordered and regulated process that is conserved among eukaryotes. The genome, packed into chromosomes, is

distributed between two daughter cells during anaphase. Cytokinesis must be spatially and temporally coordinated with sister chromatid segregation. Cytokinesis failure and the subsequent generation of aneuploidies have been associated with tumorigenesis [1]. Detailed mechanistic studies are important if we want to understand its normal cellular functions as well as its impact on human diseases.

In fungi and animal cells, the cytokinetic machinery comprises two major elements: septins and a contractile actomyosin ring. In *Saccharomyces cerevisiae*, the process takes place at the division site, a narrow region linking mother and daughter cells. At the end of G1, the Cdc42 GTPase polarizes actin cables and patches towards the new bud site, and the septin ring is assembled [2,3]. The septin ring is reorganized later in S phase and becomes an hourglass-like structure [4] that splits into two rings at anaphase [5–7]. Septin serve as an anchor for various cytokinesis-related proteins including the type II myosin heavy chain, Myo1 [8]. Myo1, together with actin filaments and the essential and regulatory myosin light chains Mlc1 and Mlc2, shape the actomyosin ring (AMR)[5,8–10]. The AMR leads to the furrow ingression as a consequence of the contraction and constriction of the Myo1-actin layer [11,12].

At the AMR localize some regulators of the cytokinesis as Iqg1 and Hof1, which, in turn, promotes the recruitment of Inn1 and Cyk3 [6,13–15]. These proteins are part of the Ingression Progression Complexes (IPCs)[16,17], which mediate the activation of the chitin synthase Chs2 [6,16,18,19]. Chs2 synthesizes the primary septum (PS) concomitantly with the AMR constriction [20,21]. Primary septum formation is tightly coupled to actomyosin ring contraction and ingression of the plasma membrane at the division site [22]. The IPCs form the central machinery required to coordinate those cytokinetic events [16]. Defects associated with one of the processes can perturb the others [18,23–25].

Once PS has been synthesized, the two secondary septa (SS) will be formed by Chs3, glucan synthases (Fks1) and mannosyltransferases on both sides of the PS [21,26,27]. Finally, cytokinesis is completed when the daughter cell synthesizes hydrolases and chitinases to hydrolyze the remaining cell wall structures in between the SS [28].

We know little about what regulates the timing of cytokinesis, and the mechanism ensuring it only happens after anaphase is complete is poorly understood. Anaphase is regulated by two pathways: FEAR (cdcFourteen Early Anaphase Release) and MEN (Mitosis Exit Network). Both are coordinated to promote the activation of the Cdc14 phosphatase [29–32]. Cdc14 is responsible for Cdk1 (Cdc28 in budding yeast) inactivation and the dephosphorylation of Cdk1 targets during mitosis [33]. Several MEN kinases have been found to be involved in cytokinesis [34]. Polo-like kinase, Cdc5 regulates AMR formation and membrane ingression [35,36]. Dbf2, the downstream MEN kinase, phosphorylates Hof1 promoting its mobilization from the septins to the AMR [7,35]. By contrast, Cdc28-Clb2 inhibits AMR formation and contraction by delaying Hof1 localization at the AMR [37], limiting the actin recruitment by Iqg1, and keeping Chs2 at the endoplasmic reticulum (ER). Chs2 translocates to the division site upon Chs2 dephosphorylation by Cdc14 [38,39]. Cdk1 also inhibits Iqg1 and Inn1 localization at the division site, and Inn1 interaction with IPCs [37,40,41]. However, the inactivation of Cdc28-Clb2 activity during late anaphase is not sufficient to trigger cytokinesis [39,42],it is also necessary the Cdc14-dependent dephosphorylation of Iqg1, Inn1 and Chs2 for cytokinesis completion [39,41,43,44]. However, recent work demonstrates that multiple phosphatases shape the phospho-proteome during mitotic exit [45,46], pointing out

105 to the redundant contribution of other phosphatases such as PP2A$^{Rts1}$ and PP2A$^{Cdc55}$
106 with Cdc14 [45]. These observations suggest that PP2A phosphatases could also be
107 required for cytokinesis.
108
109 PP2A$^{Cdc55}$ is a family of serine/threonine phosphatases conserved throughout
110 eukaryotes. It is found as a heterodimer or heterotrimer composed of a scaffold
111 subunit (Tpd3 in yeast), a catalytic subunit (Pph21/22) and a regulatory subunit
112 (Cdc55 or Rts1)[47,48]. The regulatory subunit confers substrate specificity and
113 regulates the phosphatase subcellular localization. PP2A$^{Cdc55}$ regulates the cell cycle
114 in different ways: it controls bud polarization and cell wall synthesis [49,50], prevents
115 sister chromatid separation [51], regulates the entry into mitosis [52,53] and the
116 spindle assembly checkpoint [54], dephosphorylates Net1 during mitosis [55,56], and
117 keeps MEN inhibited by dephosphorylating Bfa1[57].
118
119 MEN and Cdc14 phosphatase initiate cytokinesis by counteracting Cdk1
120 dephosphorylation in budding yeast [44]. Here, we propose that a second
121 phosphatase, PP2A$^{Cdc55}$, regulates cytokinesis through the dephosphorylation of IPC
122 proteins. We have found that the PP2A$^{Cdc55}$ participates in the regulation of the
123 phosphorylation state of Hof1, Inn1, Cyk3 and Chs2 *in vivo* and dephosphorylates
124 Hof1 and Chs2 *in vitro*. Interestingly, *cdc55*Δ mutants are defective in AMR
125 contraction and Primary and Secondary Septa formation, supporting a role for
126 PP2A$^{Cdc55}$ regulating cytokinesis. In the absence of Cdc55, AMR collapses in one
127 side of the division site and the PS formation occurs asymmetrically only on one side
128 of the bud neck. In conclusion, PP2A$^{Cdc55}$ coordinates AMR contraction and PS
129 formation via the dephosphorylation of IPC proteins during cytokinesis.

## Results

### PP2A$^{Cdc55}$ regulates the dephosphorylation of IPC proteins

In a previous SILAC-based phosphoproteomics analysis performed in our laboratory we identified two IPC proteins, Iqg1 and Inn1, that were hyperphosphorylated in the absence of Cdc55, suggesting that they could be dephosphorylated by PP2A$^{Cdc55}$ [58]. We envisaged that PP2A$^{Cdc55}$ may have a role during cytokinesis being the dephosphorylation of the IPC proteins the possible link between PP2A$^{Cdc55}$ and cytokinesis. This prompted us to confirm a possible regulation of the IPC proteins by PP2A$^{Cdc55}$.

It has previously been reported that mutants in the IPC subunits, for instance, *hof1*Δ and *cyk3*Δ, are synthetic lethal (SL)[59]. For this reason, we investigated the genetic interactions between *cdc55*Δ and IPC mutants. We tried to prepare double-deletion mutants with *cdc55*Δ and the non-essential IPC genes, *cyk3*Δ and *hof1*Δ, but the diploid cells did not sporulate and we were unable to obtain tetrads. Adopting another approach, we prepared double mutants with *cdc55*Δ and degron-conditional mutants to induce protein degradation for the IPC subunits [16,60]. We observed no differences in cell growth among the different mutant strains on control plates compared with WT cells (Fig. 1a). However, the viability of the double mutants, *cdc55*Δ *hof1-aid* and *cdc55*Δ *td-cyk3-aid*, was impaired under restrictive conditions (presence of auxin) compared with single mutants (Fig. 1a). The synthetic sick interactions found between *cdc55*Δ and *hof1-aid* or *td-cyk3-aid* degron mutants indicate that Cdc55 is functionally related to the IPC subunits, Hof1 and Cyk3, and suggest that Cdc55 could regulate the function of Hof1 and Cyk3.

To study the functional link between Cdc55 and the IPCs, we studied whether $PP2A^{Cdc55}$ regulates the dephosphorylation of IPC proteins. We analyzed the phosphorylation status of the IPC proteins Myo1, Iqg1, Hof1, Cyk3 and Chs2 in the absence of Cdc55 during cytokinesis. To analyze the phosphorylation of the proteins during cytokinesis, we synchronized cells at metaphase and released them synchronously into anaphase in order to visualize the phosphorylation of the IPC proteins during anaphase. Cells were arrested in metaphase by the depletion of the APC coactivator Cdc20 under the control of the methionine-responsible *MET3* promoter and released them into anaphase by re-introduction of Cdc20. The phosphorylation level of the IPC proteins was determined using Phos-tag™ gels. DNA content measured by flow-cytometry and mitotic spindle staining determined by tubulin immunofluorescence were used as markers of cell-cycle progression. Cdc14 release from the nucleolus was also determined as control of mitosis progression. Cdc14 was prematurely release in metaphase in absence of Cdc55 as previously published [56].

A unique Myo1 band was resolved in the protein gel in WT and *cdc55*Δ cells, (Fig. S1a). Therefore, no phosphorylation isoforms were detected for Myo1 during anaphase, at least as far as it could be detected by western blot analysis. Next, we analyzed the phosphorylation pattern of Iqg1. It was suggested that Iqg1 is phosphorylated by Cdk1, since its localization and function depend on the Cdk1-phosphorylation sites [40,43]. However, Iqg1 phosphorylation levels during the cell cycle have not previously been reported. Here, we show how Iqg1 is phosphorylated and dephosphorylated during progression through mitosis. In wild-type cells, Iqg1 was phosphorylated in metaphase, became dephosphorylated during anaphase (Fig.

S1a 20-30 min) and was quickly phosphorylated in telophase/cytokinesis (Fig. S1a 40-50 min). In *cdc55*Δ mutant cells, the dephosphorylation events in anaphase and cytokinesis were observed although with lower efficiency than in WT cells (Fig. S1a, 40-70 minutes). While Iqg1 phosphorylation was higher in *cdc55*Δ mutant cells during anaphase compare to WT cells, the slight differences observed between WT and *cdc55*Δ cells in cytokinesis are not significant enough to conclude that there is an increase in Iqg1 phosphorylation in the absence of Cdc55.

Subsequently, in wild-type strains, we observed that Hof1 and Inn1 were phosphorylated after 30 min, corresponding to the time of anaphase (Figs. 1b and c). This phosphorylation is involved in the regulation of both proteins [37,41,61]. After anaphase, Hof1 and Inn1 are quickly dephosphorylated. Cdc14 dephosphorylates Inn1 [41], but to our knowledge no phosphatase has been described in the context of Hof1 dephosphorylation. In *cdc55*Δ cells, although slower-migrating isoforms of Inn1 and Hof1 were detected, the phosphorylation levels were similar to WT cells during metaphase and early anaphase. While anaphase hyperphosphorylation occurred normally, interestingly, Hof1 and Inn1 remained hyperphosphorylated during late anaphase and cytokinesis, unlike the control cells (Figs. 1b and c, 50-90 min). These results suggest that $PP2A^{Cdc55}$ participates in the dephosphorylation of Inn1 and Hof1 during late anaphase/cytokinesis.

Cyk3 has recently been reported to be phosphorylated upon MEN activation concomitantly with Hof1 [19]. In control cells, Cyk3 started to be phosphorylated in anaphase (Fig. 1d, 30 min) and this phosphorylation was maintained until G1. In *cdc55*Δ mutant cells, on the other hand, the phosphorylation was already present in

metaphase and increased at anaphase (Fig. 1d; 40 min), indicating that Cyk3 is slightly hyperphosphorylated in the absence of Cdc55 during anaphase. Although the Cyk3 phosphorylation during cytokinesis was similar in presence and absence of Cdc55. This result suggests that $PP2A^{Cdc55}$ might control the state of phosphorylation of Cyk3, especially during mitosis but not during cytokinesis. Finally, the state of Chs2 phosphorylation was analyzed as the final IPC effector. Chs2 presented many different migrating bands and it was described that Chs2 has different post-translational modifications. For this reason, we performed an alkaline phosphatase experiment to check which correspond to phosphorylations (Fig. S1b). In presence of alkaline phosphatase, the slower Chs2 migrations bands collapse into the faster migration band indicating that mostly the upper bands are phosphorylation events. Chs2 protein presented slow migration isoforms during metaphase and early anaphase in control cells (Fig. 1e meta-20 min). Chs2 phosphorylation in metaphase is important for retaining Chs2 in the ER [38,39,62]. From anaphase until early G1 (Fig. 1e; 30-50 min), Chs2 faster migration isoforms were detected with slower-migrating isoforms accumulating again later on (Fig. 1e; 60-90 min). Remarkably, in *cdc55*Δ mutant cells the slower-migrating isoforms are detectable throughout the time-course, indicating that Chs2 was not efficiently dephosphorylated during late anaphase/cytokinesis (Fig. 1e; 40-70min). We can conclude that Chs2 phosphorylation levels are altered in the absence of Cdc55 during cytokinesis.

The previous results suggest that $PP2A^{Cdc55}$ phosphatase counteracts Hof1, Inn1, Cyk3 and Chs2 phosphorylation. To determine whether these IPC proteins are $PP2A^{Cdc55}$ substrates, we examined whether they physically interact with Cdc55 by

carrying out co-immunoprecipitation experiments. In Cdc55 immunoprecipitates, from cells released into synchronous anaphase by Cdc20 depletion and re-induction, we detected co-purification of Cyk3, Inn1, Hof1, and Chs2 during anaphase and cytokinesis (Fig. 1f). These results indicate that $PP2A^{Cdc55}$ and Cyk3, Inn1, Hof1, and Chs2 could physically interact and that these interactions would occur during progression through mitosis and cytokinesis. Taken together, these results suggest that Cyk3, Inn1, Hof1, and Chs2 are likely to be an *in vivo* substrate of $PP2A^{Cdc55}$.

## $PP2A^{Cdc55}$ dephosphorylates Hof1 and Chs2 *in vitro*

To explicitly test whether Inn1, Hof1, Cyk3 and Chs2 are direct $PP2A^{Cdc55}$ dephosphorylation targets, we measured $PP2A^{Cdc55}$ *in vitro* phosphatase activity in assays after Cdc55 immunopurification from metaphase-arrested cells when $PP2A^{Cdc55}$ is active [56]. The substrates were recombinant fragments of Cyk3 (full length), Inn1 (full length), Hof1 (full length) and Chs2 (1-629) purified from *E. coli*. To perform the phosphatase assays, the substrates first had to be phosphorylated. Cdk1 and MEN kinases were used, as they are the most relevant regulatory kinases of the IPC [35,37,61]. Unfortunately, no Cyk3 phosphorylation was observed in kinase assays using Clb2-Cdk1, Cdc5, Cdc15, and Dbf2 as kinases. Therefore, no phosphatase assay for Cyk3 could be performed. A weak Inn1 phosphorylation event was observed in Clb2-Cdk1 kinase assays after very long exposure times (Fig. S2a). However, this Inn1 phosphorylated substrate did not have enough signal to be able to proceed with the phosphatase assay. Clb2-Cdk1, Cdc5, and Dbf2 are known to phosphorylate Hof1 [7,35], so we phosphorylated Hof1 with the three kinases. However, we only detected Hof1 phosphorylation in Clb2-Cdk1 kinase assays (Fig. S2b). Finally, Chs2 kinase assays were performed with Clb2-Cdk1 and Dbf2 and

Chs2 was phosphorylated with both kinases (Fig.S2c) as previously described [38,39,63].

*In vitro* $^{32}$P-phosphorylated Hof1 and Chs2 were used as substrates for the phosphatase assays. Cdc55 immunoprecipitates were incubated with these substrates and the reduction of $^{32}$P-phosphorylated proteins was determined. Clb2-Cdk1-phosphorylated Hof1 and Chs2 and Dbf2-phosphorylated Chs2 were incubated with the Cdc55 immunoprecipitates from control cells expressing Cdc55 and a *cdc55-ED* inactive version of PP2A$^{Cdc55}$ [64] from metaphase-arrested cells. Using Hof1 as a substrate, Hof1 phosphorylation signal intensity was statistically significant reduced by 59% in the assay with PP2A$^{Cdc55}$ (Fig. 2a). By contrast, Hof1 was not dephosphorylated in the inactive-version PP2A$^{cdc55\text{-}ED}$ (Fig. 2a). These results demonstrate that PP2A$^{Cdc55}$ dephosphorylates Hof1 *in vitro*, confirming that Hof1 is its substrate. To our knowledge, this is the first time a phosphatase has been described to dephosphorylate Hof1.

When using Chs2 as a substrate, the PP2A$^{Cdc55}$ phosphatase assays for Cdk1- and Dbf2-phosphorylated Chs2 showed a strong decrease in the Chs2 phosphorylation signal (Fig. 2b). A reduction of 84% in the Chs2 phosphorylation signal was noted in the case of Cdk1-phosphorylated Chs2 and a 38% reduction in Dbf2-phosphorylated Chs2, reflecting the higher dephosphorylating ratios for Cdk1-phosphorylated residues. The *cdc55-ED* mutant version was not able to dephosphorylate any phosphorylated Chs2 significantly. These results strongly suggest that Chs2 is dephosphorylated *in vitro* by PP2A$^{Cdc55}$, confirming that Chs2 is also a PP2A$^{Cdc55}$ substrate.

In conclusion, the phosphatase assays indicate that $PP2A^{Cdc55}$ counteracts phosphorylation in Hof1 and Chs2, reinforcing the idea that they are direct $PP2A^{Cdc55}$ substrates. $PP2A^{Cdc55}$ is known to counteract Cdk1 phosphorylation, but this is the first time, to our knowledge, that a Dbf2 substrate has been shown to be dephosphorylated by $PP2A^{Cdc55}$.

**Defective septum formation in the absence of Cdc55**

Based on the multi-nuclear phenotype of the *cdc55*Δ deletion mutant at low temperatures, it has been suggested that $PP2A^{Cdc55}$ phosphatase is involved in cytokinesis [47]. This prompted us to study the cytokinesis phenotypes of the *cdc55Δ* mutant cells.

Septins are GTP-binding proteins that act as scaffold platforms for many proteins and impose a diffusion barrier for regulating cell polarity, cell remodeling and cytokinesis. Septins are recruited at the bud site during late G1 [65,66]. Upon assembly, they form a ring-like structure at the division site. This structure has a dynamic septin organization that becomes stabilized when the definitive collar or hourglass-like structure is acquired during late anaphase [4]. This collar becomes reorganized into two rings at the onset of cytokinesis [67,68]. Once cytokinesis is completed, and just before next cycle septins are recruited, septins are disassembled from the division site [4,65,69]. We wondered whether septin structures were defective in the absence of Cdc55. Septins were visualized *in situ* by immunofluorescence staining of Cdc11 and Shs1-HA in asynchronous cells. The septin structures, septin rings, collar and double rings, were indistinguishable between *cdc55Δ* and wild-type cells (Fig. S3), suggesting that septin dynamics might not be greatly affected by the absence of Cdc55.

304

305 PP2A$^{Cdc55}$ is involved in bud morphology through actin polarization and cell-wall
306 synthesis [50]. Polarized growth must be temporally coordinated with the events of
307 the cell cycle. Actin cytoskeleton polarization at the site of bud emergence is
308 triggered at Start by the kinase activities of Cln1,2-Cdc28. In addition, Clb2-Cdc28
309 restrains repolarization to the mother bud neck [70]. Only when the Clb2-Cdc28
310 kinase is inactivated at the end of mitosis, the actin cytoskeleton is directed to the
311 neck to complete cytokinesis. Actin is then recruited in an Iqg1-dependent manner to
312 the division site and it is essential for the formation of the AMR [9,43]. We envisage
313 the possibility that PP2A$^{Cdc55}$ affects actin cytoskeleton polarization, not only during
314 the period of apical growth, but also at the end of mitosis. For this reason, we
315 wondered whether actin polarization was defective in *cdc55*Δ cells. To examine this
316 possibility, actin filaments were stained with rhodamine-labelled phalloidin in cells
317 progressing through mitosis and cytokinesis. Actin signal was found to be
318 depolarized in metaphase-arrested cells both in the wild-type and *cdc55Δ* strains, as
319 expected (Fig. S4a). When cells completed mitosis, wild-type cells polarized the
320 actin cytoskeleton to the division site. In *cdc55Δ* mutants, actin was also repolarized
321 in a timely manner at the division site during cytokinesis (Fig. S4a). However, in a
322 subpopulation of *cdc55Δ* cells, actin polarization at the new bud was observed
323 before cytokinesis had been completed (Fig. S4b). We were able to observe actin
324 signals simultaneously at the division site during cytokinesis and at the new bud site
325 in 12.5% of *cdc55Δ* mutant cells, whereas there was no premature actin
326 repolarization at the new bud site in wild-type cells (Fig. S4b). The premature actin
327 localization indicates that actin re-polarization of the next cell cycle occurs before cell

division in a fraction of *cdc55Δ* cells. Therefore, $PP2A^{Cdc55}$ could act to prevent actin re-polarization until cytokinesis is completed.

Cytokinesis in budding yeast is accomplished by the concerted action of the actomyosin contractile ring (AMR) and the formation of the septum. We investigated how these two processes occur in the absence of Cdc55. First, to clarify whether the actomyosin contractile ring is functional, we analyzed the localization of a Myo1-tdTomato fusion protein in cells progressing through mitosis and cytokinesis by the synchronous release from the metaphase arrest by Cdc20 depletion. It has been described that Myo1 localizes to the division site immediately after budding, so in metaphase-arrested cells Myo1-tdTomato was localized at the bud neck in control cells. Similarly, Myo1-tdTomato was detected at the bud neck at metaphase in *cdc55Δ* strains. The signal size is reduced during anaphase, reflecting the contraction of the AMR, until the signal becomes a single dot and finally disappears (Fig. 3a). The dynamics of AMR contraction are similar in the two strains (6 minutes from the start of contraction to the disappearance of the signal), but the “dot” signal collapsed to one side of the division site in almost all the *cdc55Δ* cells (Fig. 3b *cdc55Δ*). We observed that the AMR contraction was asymmetric with respect to the centripetal axis in 96% (N=30) of *cdc55Δ* cells (Fig. 3b). In order to check whether the asymmetric Myo1 signal is not due to an adaptive mechanism of the *cdc55Δ* deletion mutant cells, we investigated the Myo1 contraction after inducing the Cdc55 degradation during metaphase using an auxin-degradation system[71]. We observed that after the degradation of Cdc55, Myo1 contraction was asymmetric (86% of cells) as in *cdc55Δ* cells (Fig. 3c). The results indicate that the lack of $PP2A^{Cdc55}$ activity promotes the asymmetric contraction of Myo1.

We next examined whether Myo1 asymmetry could also be detected in the inactive version of Cdc55 (*cdc55-ED*). We synchronized cells at the metaphase-anaphase transition by Cdc20 depletion and analyzed the contraction of the Myo1-tdTomato after the release. We observed that 65% of *cdc55-ED* mutant cells showed an asymmetric Myo1-tdTomato signal upon contraction (Fig. 3c). This result indicates that, similar to the absence of Cdc55, the non-functional Cdc55 results in the alteration of AMR contraction. Overall, we conclude that Myo1 recruitment and time of localization at the division site are not altered in the absence of Cdc55, although AMR contraction is defective in the absence of $PP2A^{Cdc55}$ activity. This asymmetric localization has been reported before in some IPC mutants [25] and suggests a dysfunctional AMR. These results demonstrate that $PP2A^{Cdc55}$ is required for the correct function of AMR and for an efficient cytokinesis.

To confirm that the asymmetric AMR contraction phenotype was not affected by the tdTomato-tagging or the synchronization method, we compared fixed *cdc55Δ* cells tagged with Myo1-GFP upon release from metaphase-arrested cells by Cdc20 depletion with *cdc55Δ* cells tagged with Myo1-tdTomato synchronizing cells with alpha factor in G1. The *cdc55Δ* Myo1-GFP tagged cells showed an asymmetry of 87.5% of the population (N=23) (Fig. S5), representing a similar phenotypic penetrance to that of Myo1-tdTomato in *cdc55Δ* cells. This asymmetry was not observed in WT cells (1 asymmetric cell in the 41 cells studied).

Next, we performed the assay synchronizing cells in G1 by alpha factor in absence of Cdc55. *cdc55*Δ cells enter mitosis with a delay due to compromised Cdk1 activity because of inhibitory Cdc28-Y19 phosphorylation [72]. To correct for this delay, we introduced the *cdc28_Y19F* allele, which is refractory to Cdk1 inhibition. The *cdc55Δ*

cells containing *cdc28_Y19F* progressed normally through mitosis upon release from metaphase-arrested cells [56]. Again, we observed that Myo1-tdTomato constriction was asymmetric in 80% of the *cdc55Δ cdc28_Y19F* cell population (Fig. S5). Therefore, the asymmetric Myo1 signal in the absence of Cdc55 was observed independently of the epitope and the synchronization method used.

Then, chitin deposition in the neck was analyzed by *in vivo* staining with calcofluor white (a molecule that binds to chitin while it is being incorporated to the cell wall) and measured the fluorescence intensity of the incorporated calcofluor on living cells containing Myo1-tdTomato as a control of cytokinesis progression. We arrested cells at metaphase by Cdc20 depletion and released them into mitosis and took images 30-45 min after the release when we found cells at cytokinesis. Calcofluor intensity was then measured and quantified in wild-type and *cdc55Δ* cells (Fig. 3d). There was a statistically significant reduction of the 45% in the intensity of the calcofluor staining in the absence of Cdc55 compared with control cells. Chitin is incorporated in primary septa (PS) and secondary septa (SS), so we cannot distinguish at which of them this reduction occurs. For this reason, we repeated the calcofluor staining in cells containing a deletion of *CHS3*, the chitin synthase responsible for secondary septum formation [21]. A reduction of 70% in the calcofluor intensity was observed in the absence of Cdc55 relative to control cells (Fig. 3d). The above results suggest that primary and secondary septum formation is reduced in cells lacking $PP2A^{Cdc55}$ activity. Our results suggest that, similar to IPCs, $PP2A^{Cdc55}$ has a role coordinating AMR contraction with septum formation, probably by dephosphorylating IPC components.

To determine whether ingression of the plasma membrane could occur in *cdc55Δ* cells, we performed time-lapse video microscopy of cells expressing Myo1-tdTomato to follow AMR contraction, and the small G-protein Ras2 fused to 3 copies of GFP to study plasma membrane dynamics. The visualization of the plasma membrane at the site of division revealed no cytoplasm connection between mother and daughter cells, confirming that cytoplasmic division had been completed in control and *cdc55Δ* cells (Fig. S6). In conclusion, *cdc55Δ* cells have a defective AMR "collapsed" to one side of the division site and a reduction in septum formation, but nevertheless manage to complete cell division.

To confirm the defects in septum formation we investigated the cytokinetic structure by transmission electron microscopy (TEM). We synchronized cells at the metaphase-anaphase transition by Cdc20 depletion and captured images 40-50 mins after metaphase release. Cells synthesizing the primary septum were identified and the structure of the septum was then examined. In wild-type cells, we observed that the PS formed on both sides of the membrane invagination (Fig. 4a), as expected. Once the PS was finished, the two SS was formed on both sides of the PS (Fig. 4b). Finally, the PS is degraded, and the cells physically separated (Fig. 4c). Conversely, in *cdc55*Δ cells, the PS formed on only one side of the division site (Fig. 4d). From the cells performing primary septum formation, we quantified 85% (N=25) with asymmetric PS in absence of Cdc55. Some cells showed aberrant, thicker structures with diverse morphologies that resemble the remedial septa (Fig. 4e). The remedial septa were first described in IPC mutant cells, i.e., *myo1*Δ and *chs2*Δ [23]. They are chitin structures reminiscent of SS that allow cells to complete cytokinesis

when the PS is defective [23,73]. Strikingly, in *cdc55*Δ cells, the mother and daughter cells are finally able to separate physically upon formation of the remedial septum.

To confirm that *cdc55*Δ cells can synthesize the remedial septa as a rescue mechanism to complete cell division, we repeated the experiments against a *chs3*Δ background in which no secondary septa were formed. Similar results to those of control cells containing Chs3 were obtained, whereby the *cdc55*Δ *chs3*Δ cells had asymmetric PS formation and a remedial septum was formed (Figs. 4j-l). This result suggests that remedial septum formation enables cytoplasm separation and cell division in the absence of Cdc55. The asymmetry seen in PS formation in *cdc55*Δ by EM and the asymmetric AMR contraction confirm that $PP2A^{Cdc55}$ ensures the correct coordination of the AMR contraction and PS formation.

**$PP2A^{Cdc55}$ regulates IPC symmetric localization and residence time at the division site**

IPC proteins form a complex whose function is to coordinate AMR contraction, plasma membrane ingression and PS formation [16,19]. Hyperphosphorylation of Hof1, Inn1, Cyk3, and Chs2 in the absence of Cdc55 could affect their recruitment to the division site. For this reason, we examined whether the absence of Cdc55 disturbs the IPC subunits proper or timely localization at the division site. To do this, we established the localization of the IPC subunits by time-lapse microscopy in the absence of Cdc55. We arrested cells in metaphase by Cdc20 depletion and captured images every 2 minutes after synchronous release into anaphase by Cdc20 re-induction. Since Myo1-tdTomato has no difference in protein recruitment or residence time at the division site in the absence of Cdc55, we decided to use Myo1

dynamics as the internal control for the dynamics of AMR constriction when studying the localization of the other IPC proteins.

To determine whether $PP2A^{Cdc55}$ regulates IPC localization, we used GFP-tagged IPCs strains in controls and *cdc55*Δ cells. Consistent with the results from the Myo1 protein, Iqg1, Hof1, Cyk3, Inn1, and Chs2 were contracted asymmetrically at the division site in *cdc55Δ* cells (Fig. 5a). These findings indicate that the lack of $PP2A^{Cdc55}$ activity provokes a collapse of the AMR, resulting in defective PS formation.

We then investigated the contraction and residence time of the IPC subunits. In anaphase, Iqg1-GFP was already present at the division site and Iqg1 contraction started mostly simultaneous with Myo1-tdTomato in WT and *cdc55*Δ mutant cells (Fig. S7a). Iqg1-GFP signal was also observed at similar times in WT and *cdc55*Δ cells (Fig. 5b), consistent with the Myo1 signal. No differences were observed in residence time at the bud neck in both strains, despite the higher dispersion of the values for the *cdc55*Δ mutant (Figs. 5b and S7a). These results indicate that Iqg1 residence time is mostly normal in the absence of Cdc55.

Hof1-GFP was localized at the division site in metaphase cells as previously described [61]. In the main population of WT and *cdc55*Δ cells, the start of contraction was similar between Hof1 and Myo1(Fig. S7b), indicating that the onset of contraction was normal in the absence of Cdc55. By contrast, we observed that the Hof1-GFP signal took longer to complete contraction and to disappear in *cdc55*Δ than it did in WT cells (Figs. 5b and Fig. S7b). We conclude that the absence of Cdc55 increases the residence time of Hof1 signal at the division site, further

demonstrating that cytokinesis is affected. The longer Hof1 localization at the division site is consistent with the collapsed AMR and the asymmetry of the IPC components.

The Cyk3-GFP signal appeared at the division site 0-2 minutes after the Myo1-tdTomato signal started to contract in WT and *cdc55*Δ cells, but the Cyk3 signal remained longer at the division site in the absence of Cdc55 (Figs. 5c and S7c). These results suggest that Cyk3 localization dynamics are regulated by $PP2A^{Cdc55}$.

On the other hand, Inn1-GFP appeared at the division site when Myo1-tdTomato started to contract in WT and *cdc55*Δ cells. The Inn1-GFP signal was detected at similar time in the WT and *cdc55*Δ mutant cells (Figs. 5c and Fig. S7d). We conclude that Inn1 contraction and residence time are not affected in absence of Cdc55.

Similar to Hof1 and Cyk3, the Chs2-GFP residence time in *cdc55Δ* mutant cells was longer. Chs2-GFP was recruited at the division site when the AMR started to contract in both WT and *cdc55Δ* cells. Conversely, the Chs2 signal lasted longer at the division site in *cdc55Δ* cells (Figs. 5c and S7e). Therefore, Cdc55 absence interferes with Chs2 contraction and its residence time at the division site. We can conclude that $PP2A^{Cdc55}$ is required for proper Chs2 localization dynamics.

**Timely Chs2 dephosphorylation by PP2A-Cdc55 is required for proper AMR contraction**

Our results suggest that Cdc55 regulates Hof1 and Chs2-dependent processes during cytokinesis, and that these proteins are Cdc55 substrates. To screen for new

PP2A$^{Cdc55}$ substrates during mitosis, we previously performed a global study of the PP2A$^{Cdc55}$ phosphoproteome by a quantitative phosphoproteomic analysis based on SILAC labeling [58]. Wild-type cells were labeled using $^{13}C_6$-lysine and $^{13}C_6$-arginine (heavy), and *cdc55*Δ mutant cells were grown in the presence of unmodified arginine and lysine (light). Cells were arrested in metaphase and protein extracts were prepared. Phosphopeptides were enriched by TiSH-based enrichment. Phosphopeptide analysis of the heavy/light-labelled cells was done by LC-MS/MS. The screening revealed that a phosphopeptide corresponding to Chs2 protein was hyperphosphorylated in *cdc55*Δ mutant cells. The Chs2 peptide contained one Cdk1 minimal S/TP site: S133 (Figure 6a). The phosphosite was detected with the highest confidence (pRS site probability 99.9% and p-value < 0.00001) and was also identified in a second phospho-proteomic study for *cdc55*Δ mutant cells [46]. This result confirms that Chs2 is a PP2A$^{Cdc55}$ substrate. The S133 is one of the 6 Cdk1 consensus sites (S/T-P) previously reported to be phosphorylated by Cdk1 [74]. In addition, Chs2 S14, S60, S69 and S100 can be efficiently dephosphorylated by Cdc14 while the other two sites S86 and S133 can also be dephosphorylated by Cdc14 although less efficiently [39]. It is important to remember that Cdc14 is prematurely release from the nucleolus and active as a phosphatase in *cdc55*Δ mutant cells [56,57]. Therefore, despite the fact that the two phosphatases can contribute to the dephosphorylation of Chs2, in the phosphoproteomic analysis the identification of a hyperphosphorylated peptide in absence of Cdc55 implies that this site is not mainly affected by Cdc14 (the phosphosites mainly dephosphorylated by Cdc14 will be identified as hypophosphorylated since Cdc14 is prematurely active in *cdc55*Δ cells). To advance in the mechanistic understanding of the role of PP2A$^{Cdc55}$

in cytokinesis we prepared phospho-mutants for Chs2 and determined the phenotypic effects of these mutations.

To demonstrate that the cytokinetic defects observed in *cdc55*Δ mutant cells were due to the increase of Chs2 phosphorylation levels, we introduced the *chs2-6A-YFP* mutant, were all the SP sites were mutated to alanine [75], in *cdc55*Δ mutant cells. Myo1 and Chs2 signals were asymmetric in the presence of the control *CHS2-YFP* (79% of cells; N=13) in absence of Cdc55, as expected (Fig. 6b) Remarkably, in the *chs2-6A-YFP* non-phosphorylable version Myo1 and Chs2 localization became symmetric in 78% of cells (N=18), indicating that the non-phosphorylable *chs2-6A* mutant rescued the asymmetric localization of Myo1 in *cdc55*Δ mutant cells (Fig. 6b). The Chs2-YFP signal was detected earlier at the bud neck, probably due to the overexpression of Chs2, but the Myo1 and Chs2 contraction time were similar in the presence of Chs2 and *chs2-6A* (Fig. 6c). We can conclude that timely dephosphorylation of Chs2 by PP2A-Cdc55 is required for proper AMR contraction.

These findings demonstrate that the lack of $PP2A^{Cdc55}$ activity provokes a collapse of the AMR, representative of a dysfunctional AMR, and that it also alters the residence time at the division site of IPC proteins. Therefore, $PP2A^{Cdc55}$ dephosphorylation of the IPC subunits is essential for maintaining proper AMR contraction and septum formation; both required for an efficient cytokinesis.

## Discussion

### $PP2A^{Cdc55}$ regulates IPC phosphorylation and its localization dynamics at the division site

The localization and function of the IPC components (Iqg1, Myo1, Hof1, Cyk3, Inn1, and Chs2 proteins), which coordinate AMR contraction, plasma membrane ingression and PS formation, are tightly regulated by phosphorylation. To date, only two phosphatases, Cdc14 and $PP2A^{Rts1}$, are known to have a role in cytokinesis [76], being just Cdc14 described to dephosphorylate some of the IPC proteins [39,41–43]. A putative role for $PP2A^{Cdc55}$ in cytokinesis was proposed because of its elongated morphology and multinucleated cells at low temperatures in *cdc55*Δ cells [47]. In addition, $PP2A^{Cdc55}$ is localized at the division site during cytokinesis [77]. However, the role of $PP2A^{Cdc55}$ during cytokinesis was not demonstrated and the molecular mechanism by which $PP2A^{Cdc55}$ regulates cytokinesis is still unknown. Here, we describe a new function of $PP2A^{Cdc55}$ phosphatase in the regulation of cytokinesis. In summary, $PP2A^{Cdc55}$ regulates the dephosphorylation of IPC and is involved in proper AMR contraction and septum formation. $PP2A^{Cdc55}$ dephosphorylates Hof1 and Chs2 *in vivo* and *in vitro*, indicating that they are direct $PP2A^{Cdc55}$ targets. In addition, $PP2A^{Cdc55}$ also participates in the regulation of Cyk3 and Inn1 phosphorylation. The defects seen in IPC residence time and asymmetric localization in the absence of Cdc55 may be a direct consequence of its own phosphorylation regulation by $PP2A^{Cdc55}$ or a secondary effect of the other IPC dephosphorylation by $PP2A^{Cdc55}$. Both scenarios are plausible given that we demonstrated that at least two proteins, Hof1 and Chs2, are direct targets of $PP2A^{Cdc55}$. In the case of Chs2, we have been able to demonstrate that the defects of AMR contraction in absence of Cdc55 are due to the increased levels of Chs2 phosphorylation, since the *chs2-6A* non-phosphorylable mutant rescue the asymmetric Myo1 signal in *cdc55* mutant cells. This result suggests that timely dephosphorylation of Chs2 by $PP2A^{Cdc55}$ is crucial for proper AMR contraction. Since

575 the IPC coordinates AMR constriction, plasma membrane ingression and septum
576 formation, we propose that PP2A$^{Cdc55}$ is also involved in this efficient mechanism of
577 coordination through IPC dephosphorylation (Fig. 7).
578
579 **The role of PP2A$^{Cdc55}$ during cytokinesis**
580 In the absence of Cdc55, Myo1 was constricted and unanchored in a timely fashion,
581 but the constriction was displaced from the central axis, becoming asymmetric (Figs.
582 3a and S5). This phenotype is characteristic of IPC mutants [6,25,67] and denotes a
583 dysfunctional AMR.
584 Consistent with this, Iqg1, Cyk3, Hof1, Inn1, and Chs2 localization were also
585 asymmetric upon AMR constriction (Fig. 5a). The asymmetric Cyk3 and Inn1
586 localization have also been described in *hof1*Δ mutants [13,19]. Hof1
587 dephosphorylation by PP2A$^{Cdc55}$ (Fig. 1b) may contribute to Hof1 functionality and to
588 regulate Cyk3 residence time and asymmetry at the division site. On the other hand,
589 Hof1 asymmetry was already described in *chs2*Δ cells [6]; but not *vice versa* [6,16].
590 Therefore, PS formation by Chs2 influences Hof1 constriction. Consequently,
591 PP2A$^{Cdc55}$ could regulate Hof1 constriction directly and/or through PS regulation,
592 since both Hof1 and Chs2 are PP2A$^{Cdc55}$ substrates. Defective PS formation could
593 also contribute to the asymmetry seen in the IPC proteins.
594
595 PP2A$^{Cdc55}$ also regulates septum formation. Chitin incorporation was decreased in
596 the *cdc55*Δ and *cdc55*Δ *chs3*Δ cells (Fig. 3d), indicating that Chs2 activity might be
597 impaired. The electron microscopy study of septum formation demonstrated that PS
598 is still formed in *cdc55*Δ cells, being predominantly asymmetric on one side of the
599 division site during its formation (Figs. 4d, j). PS was reported to be asymmetric in

600 around 50% of *hof1*Δ mutant cells [35]; while more than 80% of the cells showed
601 asymmetric PS in *cdc55*Δ cells. This difference in magnitude can be explained taking
602 into consideration that at least two IPC, Chs2 and Hof1, are $PP2A^{Cdc55}$ substrates.
603
604 Later on, a remedial septum is formed that contains even cytosol fractions
605 embedded in the septa (Fig. 4). This remedial septum formation has been seen
606 before when PS formation is disturbed in IPC mutants [13,19,63,78] and MEN
607 mutants [37,63,78]. Chs3 is the chitin synthase, together with glucan synthases and
608 mannosyltransferases responsible for the SS formation and the construction of the
609 remedial septum [26,27,73]. However, the *chs3Δ* mutant is still viable and capable of
610 divide, suggesting that additional chitin synthases might be able to incorporate chitin
611 in the absence of Chs3. This may explain why the remedial septum is still formed in
612 the *cdc55Δ chs3Δ* double mutant.
613 In addition, Hof1 regulates the CSIII function inhibiting Chs3 activation through the
614 interaction with Chs4 [79]. Hof1 removal from the division site also dissociates Chs4,
615 allowing Chs3 activation. Therefore, the increased Hof1 residence time in the
616 absence of Cdc55 might predict an inactive Chs3 at the division site, and
617 consequently less extensive SS formation, in agreement with the results of our
618 calcofluor staining in *cdc55*Δ mutant cells.
619
620 Hof1 have been also involved in the regulation of septin organization [7,67].
621 Therefore, the defects in Hof1 localization could be a consequence or a cause of
622 defective septin function in *cdc55Δ* cells. Nevertheless, the preliminary results
623 obtained from *in situ* immunofluorescence showed no alterations in septin structures
624 in *cdc55*Δ cells. We did not detect any differences in protein levels or

phosphorylation states in Cdc11 and Shs1 in the absence of Cdc55. In addition, the dephosphorylation of septins by $PP2A^{Rts1}$ is known to be required for septin stability [76], suggesting that septins are regulated by the other PP2A regulatory subunit, Rts1.

Recently, it has been showed that multiple phosphatases shape the phospho-proteome during mitotic exit [45,46,80]. Notably, Hof1 and Chs2 phosphosites have been identified in *cdc55* and *cdc14* mutants [45]. Here, we demonstrated that Hof1 and Chs2 are $PP2A^{Cdc55}$ substrates and Cdc14 was reported to dephosphorylate Chs2 [39]; supporting a possible redundant contribution to cytokinesis of several phosphatases. Further investigations will be required to understand the coordinate regulation of the multiple phosphatases during the cell cycle.

As most cytokinesis events and proteins are conserved in higher eukaryotes, it is reasonable to suppose that our results could be translated to the mechanism regulating cytokinesis in human cells. The $PP2A^{Cdc55}$ homologue in humans, $PP2A^{B55}$, could regulate the proteins involved in the cleavage furrow and cell membrane integrity, which would help us understand the human diseases that feature altered cytokinesis.

## Materials and methods

### Yeast strains, plasmids and cell-cycle synchronization procedures

All yeast strains used in this study were derivatives of W303 and are listed in Table S1. Epitope tagging of endogenous genes and gene deletions were performed by gene targeting using polymerase chain reaction (PCR) products [81]. Cell

650 synchronization using α-factor and metaphase arrest by Cdc20 depletion and entry
651 into synchronous anaphase by Cdc20 re-introduction were performed as previously
652 described [82]. To obtain the *pGAL1-CDC55* construct, the DNA fragment containing
653 the *GAL1* promoter was cut with SpeI and subcloned into the *CDC55* containing
654 plasmid previously digested with NheI.
655 All the *cdc55*Δ mutant strains were freshly prepared by transformation or by crossing
656 strains to avoid accumulation of suppressor mutations. The introduction of the
657 cdc55Δ deletion was determined by PCR-genotyping and observation of the slow
658 growth and elongated morphology under the microscope.
659

660 **Recombinant protein purification**

661 All plasmids were freshly introduced into BL21 *E. coli*. Cells were grown in LB
662 medium and protein expression was induced with 0.1 mM isopropyl β-D-1-
663 thiogalactopyranoside (IPTG) at 25ºC overnight. Collected cells were washed with
664 PBS1 and frozen for at least 30 minutes.
665 Cells containing $His_6$-Cyk3, $His_6$-Inn1 or $His_6$-Hof1 plasmids[16] were resuspended in
666 cold lysis buffer (30 mM Tris-HCl, pH 8, 300 mM NaCl, 30 mM imidazole, 0.1%
667 NP40, 10 mM β-mercaptoethanol, 1 mM PMSF, complete EDTA-free tablet (Roche))
668 and sonicated for 6 cycles of 1 min at 25 µm amplitude. Protein extracts were
669 clarified and incubated with Ni-NTA magnetic beads (Thermo Fisher) at 4ºC for 1
670 hour. Beads were washed with 10 volumes of lysis buffer and protein eluted in PBS,
671 5 mM EDTA, 5 mM DTT, 0.1% NP40, 500 mM imidazole at 4ºC for 30-60 minutes.
672 Cells containing StreptagIII-Chs2_1-629 plasmid [16] were resuspended in cold lysis
673 buffer (50 mM Tris-HCl, pH 8.0, 10% glycerol, 0.1% NP-40, 10 mM $MgCl_2$, 300 mM
674 NaCl, 5 mM β-mercaptoethanol, 10% BugBuster® (Millipore), 1 mM PMSF, complete

675 EDTA-free tablet (Roche) containing 5 U/mL of nuclease (Pierce), incubated in a
676 rotatory wheel at 25ºC for 20 minutes. Protein extracts were clarified and incubated
677 with Strep-tactin® Superflow® resin (Iba Lifescience) at 4ºC for 1 hour. Beads were
678 washed with ten volumes of lysis buffer (without BugBuster®), and protein was
679 eluted in 50 mM Tris-HCl, pH 8.0, 10% glycerol, 0.1% NP-40, 10 mM $MgCl_2$, 150 mM
680 NaCl, 5 mM β-mercaptoethanol, 2.5 mM desthiobiotin at 4ºC for 1 hour.
681
682 **Co-immunoprecipitation, kinase assays and phosphatase assays**
683 Co-immunoprecipitation assays were performed using $10^8$ yeast cells, which were
684 resuspended in lysis buffer (50 mM HEPES-KOH, pH 7.5; 70 mM KOAc, 5 mM
685 $Mg(OAc)_2$; 10% glycerol; 0.1% Triton X-100; 8 µg/mL of protease inhibitors
686 (leupeptin, pepstatin, aprotinin), 1 mM PMSF, 1.25 mg/ml of benzamidin, 1 tablet of
687 complete protease inhibitor without EDTA (Roche); 4 mM of phosphatase inhibitors
688 (β-glycerophosphate, NaF and NEM) and 1 tablet of PhosStop (Roche). Lysates
689 obtained by mechanical lysis using glass beads in a Bertin disrupter (6 cycles of 10 s
690 at 5,000 rpm). Protein extracts were clarified by centrifugation and incubated with α-
691 Pk clone SV5-Pk1 (Serotec) and α-HA clone 12CA5 (Roche) antibodies for 1 hour.
692 Protein extracts were then incubated for 1 hour with protein A-conjugated
693 Dynabeads (Life Technologies), after which the beads were washed with lysis buffer
694 at incremental KOAc concentrations (100 mM, 120 mM, 150 mM, and 60 mM
695 NaOAc). Co-immunoprecipitated proteins were eluted with loading buffer and protein
696 co-purification was visualized by western blot.
697 For kinase assays, immunoprecipitations were performed as above and incubated
698 with α-Pk clone SV5-Pk1 (Serotec) antibody. Beads were washed with ten volumes
699 of lysis buffer and twice with the kinase reaction buffer (50 mM Tris-HCl, pH7.4, 10

mM $MgCl_2$, 1 mM DTT). The kinase reaction (50 mM Tris-HCl, pH7.4, 10 mM $MgCl_2$, 1 mM DTT, 5 mM β-glycerophosphate, 25 μM ATP, 10 mCi/mL $^{32}$gamma-ATP and 2 ng-1 μg of protein substrate (plus 2 mM EGTA for the Cdc5 kinase assay) was incubated at 30ºC for 30 minutes for 6His-Inn1, 6His-Hof1, and Streptag-Chs2, and 1 hour for 6Hys-Cyk3. Kinase assays were stopped by placing the tubes on ice. The supernatant containing the phosphorylated substrate was separated from the magnetic beads and stored at -80ºC. An aliquot of the kinase assay was mixed with SDS-PAGE loading buffer, proteins were separated by electrophoresis, transferred to nitrocellulose membranes and radioactivity detected in a Typhoon FLA950 (GE Healthcare). Immunopurified protein was quantified by western blot and the membrane was stained with Coomassie to detect the recombinant substrate. Proteins were quantified using FiJi software [83].

For phosphatase assays, cells containing $HA_3$-*Cdc55-ED* and Cdc55 were collected after arresting them in metaphase. Immunoprecipitation was performed as above, but without phosphatase inhibitors, after which, beads were washed twice with phosphatase buffer. Beads were incubated with phosphatase reaction buffer (500 mM Tris-HCl pH7.4, 1 mM EGTA, 10 mM β-mercaptoethanol, 10 mg/mL BSA; and the indicated phosphorylated substrate) at 30ºC for 30 minutes. Reactions were terminated by adding SDS-PAGE loading buffer. Proteins were separated by electrophoresis, transferred to nitrocellulose membranes and radioactivity was detected in a Typhoon FLA950 apparatus (GE Healthcare). Western blot with the membrane was then performed to analyze and quantify the amount of protein immunoprecipitated. The membrane was stained with Coomassie to detect the recombinant substrate. Proteins were quantified using FiJi software, and values of the mean and SEM calculated.

For the Chs2 alkaline phosphatase assay, metaphase arrested cells were collected and native protein extracts were prepared following the immunoprecipitation protocol. The protein extracts were incubated with alkaline phosphatase (Anthartic phosphatase, New England Biolabs) in EBX reaction buffer (50mM HEPES/KOH pH 7.5, 100mM KCl, 2.5mM $MgCl_2$, 0.25% Triton X-100, 1M DTT) with protease inhibitors (8 µg/mL (leupeptin, pepstatin, aprotinin), 1 mM PMSF, 1.25 mg/ml of benzamidin, 1 tablet of complete protease inhibitor without EDTA (Roche)) at 37ºC for 15 minutes. To inhibit the alkaline phosphatase PhosStop (Roche) was used.

**Microscopy techniques**

Synchronized cells for time-lapse experiments were deposited in chambers (Nunc Lab-Tek) containing concanavalin A/PBS 1 mg/mL. Images were captured every 2 minutes. Different z-stacks at 0.7-µm intervals were taken and projected onto a single image per channel. A Zeiss-Apotome epifluorescence microscope with an HXP 120C fluorescent lamp and a Carl Zeiss Plan-Apochromat 63x N.A 1.40 oil immersion lens were used. The filters used were Cy3, GFP, and DAPI. For the GFP-Ras2 experiments the Apotome was disabled. For the Cyk3-GFP time-lapse experiments, a Carl Zeiss LSM880 confocal microscope, with a 63x N.A. objective was used. Images were acquired using ZEN software. Images were quantified and processed using FiJi software. To determine the symmetry of the IPC proteins, the bud neck length was measured, the central point calculated and manually established whether the central point was inside (symmetry) or outside (asymmetry) the dot signal.

Calcofluor staining was performed with calcofluor white MR2 (Fluorescent brightener 28, Sigma) in living cells. Synchronized cells were incubated with 50 µg/mL

750 calcofluor upon release from the metaphase arrest. Images were acquired,
751 quantified and processed as for the time-lapse experiments.
752
753 Phalloidin staining was performed on fixed cells. Cells collected during the time-
754 course experiments were pre-fixed with PBS containing 3.7% formaldehyde and
755 0.1% Triton X-100 at 25ºC for 10 minutes. Cells were then washed with PBS1 and
756 fixed with 3.7% formaldehyde at 25ºC for 1 hour. After fixation, cells were washed
757 twice with PBS1 and sedimented onto a multi-well slide previously incubated with
758 poly-L-lysine. Cells were stained with a PBS solution containing 50 U/mL rhodamine
759 phalloidin R415 (Life Technologies) for 2 hours. Cells were washed twice with PBS1.
760 Mounting medium containing DAPI (Vectashield) was added, cells were covered with
761 a coverslip and sealed with nail polish. Images were acquired, quantified and
762 processed as for the time-lapse experiments.
763
764 For electron microscopy, cell samples were fixed with 0.2 M phosphate buffer
765 (without salts) pH 7.4, containing 2.5% glutaraldehyde at 25ºC, for 1 hour. Cells were
766 washed three times with phosphate buffer without glutaraldehyde and rinsed with
767 milliQ water and post-fixed with 1% osmium tetroxide for 2 hours. They were then
768 dehydrated in an acetone series (10%, 20%, 30%, 40%, 60%, 80%, and 100%) for
769 15-20 minutes. Ultrathin sections of 60-nm thickness were obtained using a UC6
770 ultramicrotome (Leica Microsystems, Austria) and stained with 2% uranyl acetate
771 and lead citrate. Sections were observed in a Jeol EM J1010 apparatus (Jeol,
772 Japan) and images were acquired at 80 kV with a 1k CCD Megaview camera.
773
774 **Fluorescence flow cytometry analysis (FACS)**

The DNA content of cells was measured by FACS. Cells were fixed in absolute ethanol for 5 min, centrifuged for 5 min at maximum speed and resuspended in 50 mM sodium citrate pH 7.4, containing 0.2 mg/ml RNase. Cells were incubated at 50ºC for 1 hour, before adding 1 mg/ml proteinase K, and incubating for an additional 1 hour. The same volume of 50 mM sodium citrate pH 7.4 containing 16 µg/mL propidium iodide was added. DNA content was analyzed with a flow cytometer (Gallios Beckman Coulter) running Kaluza flow cytometry software.

**Other techniques**

Protein extracts for western blots were obtained by TCA protein extraction. For the phostag gels, 10 µM Phostag (Wako) 5-8% gels containing 10 mM $MnCl_2$ were used. Protein gels were washed with 1 mM EDTA before transferring protein to remove the manganese. Antibodies used for western blots were α-HA clone 12CA5 (Roche), α-myc 9E10 (Babco), α-FLAG clone M2 (Sigma), α-Pk clone SV5-Pk1 (Serotec), α-Clb2 (y-180) sc-907 (Santa Cruz Biotechnology), α-tubulin clone YOL1/34 (Serotec), α-phosphoglycerate kinase (Life Technologies), α-HA rabbit (Sigma), α-Pgk1 (Invitrogen), and α-Chs2[16]. The secondary antibodies were: α-Mouse-HRP (GE Healthcare), α-Rabbit-HRP (GE Healthcare), and α-Goat-HRP (GE Healthcare). Antibodies used for immunofluorescence were: α-HA clone 12CA5 (Roche), α-Cdc14 (yE-17) sc-12045 (Santa Cruz Biotechnology), α-tubulin clone YOL1/34 (Serotec), and α-Cdc11 (Santa Cruz Biotechnology). The secondary antibodies were Cy3-labeled α-mouse (GE Healthcare), fluorescein-conjugated α-rat (Millipore), Cy3-labeled α-goat (GE Healthcare), red TEXAS α-rabbit (Jackson Laboratories) and 488 α-mouse (Life Technologies). Proteins were quantified using FiJi software, and values of the mean and SEM calculated.

## Statistical analysis

All experiments were done at least three times. Statistical analyses were performed with Prism5. Student's T-test was used to analyze the p-values of the different assays compared. A p-value <0.05 was considered statistically significant, p<0.0001 ****, p<0.001 ***, p < 0.01 **; p<0.05 *.

## Acknowledgements

We thank the optical and electron microscopy units of IDIBELL, the proteomic services of IDIBELL and the CCiT-UB for their support. The *cdc55-aid* mutant strain was a kind gift of Adam Rudner and the *CHS2-YFP* containing plasmids were a kind gift of Foong May Yeong. We thank all the members of our laboratory for discussing the work and for their critical reading of the manuscript. We thank CERCA Program/Generalitat de Catalunya for institutional support. Our laboratory is funded by the Spanish Ministry of Economy, Industry and Competitiveness (MINECO), which is part of the State Agency, through projects BFU2013-43132-P and BFU2016-77975-R (co-funded by the European Regional Development Fund, ERDF, a way to build Europe). ASD was supported by the grant BFU2014-58081-P from the Spanish Ministerio de Economia y Competitividad (co-funded by the European Regional Development Fund) and a grant from the Consejería de Universidades, Investigación, Medio Ambiente y Política Social del Gobierno de Cantabria.

**Author contribution:** YMR, OVC, MF and EQ performed the experiments. YMR, ASD and EQ designed the experiments and interpreted the data. YMR and EQ wrote the manuscript. All authors read and discussed the manuscript.

## Conflict of interest

The authors declare no competing interests.

## References

1. Fujiwara T, Bandi M, Nitta M, Ivanova E V., Bronson RT, Pellman D. Cytokinesis failure generating tetraploids promotes tumorigenesis in p53-null cells. Nature. 2005;437: 1043–7. doi:10.1038/nature04217
2. Okada S, Leda M, Hanna J, Savage NS, Bi E, Goryachev AB. Daughter Cell Identity Emerges from the Interplay of Cdc42, Septins, and Exocytosis. Dev Cell. 2013;26: 148–61. doi:10.1016/j.devcel.2013.06.015
3. Schneider C, Grois J, Renz C, Gronemeyer T, Johnsson N. Septin rings act as a template for myosin higher-order structures and inhibit redundant polarity establishment. J Cell Sci. 2013;126: 3390–400. doi:10.1242/jcs.125302
4. Ong K, Wloka C, Okada S, Svitkina T, Bi E. Architecture and dynamic remodelling of the septin cytoskeleton during the cell cycle. Nat Commun. 2014;5: 5698. doi:10.1038/ncomms6698
5. Lippincott J, Li R. Dual function of Cyk2, a cdc15/PSTPIP family protein, in regulating actomyosin ring dynamics and septin distribution. J Cell Biol. 1998;143: 1947–1960. doi:10.1083/jcb.143.7.1947
6. Oh Y, Schreiter J, Nishihama R, Wloka C, Bi E. Targeting and functional mechanisms of the cytokinesis-related F-BAR protein Hof1 during the cell

cycle. Mol Biol Cell. 2013;24: 1305–20. doi:10.1091/mbc.E12-11-0804

7. Meitinger F, Palani S, Hub B, Pereira G. Dual function of the NDR-kinase Dbf2 in the regulation of the F-BAR protein Hof1 during cytokinesis. Mol Biol Cell. 2013; 1–44. doi:10.1091/mbc.E12-08-0608

8. Finnigan GC, Booth EA, Duvalyan A, Liao EN, Thorner J. The carboxy-terminal tails of septins Cdc11 and Shs1 recruit myosin-II binding factor Bni5 to the bud neck in Saccharomyces cerevisiae. Genetics. 2015;200: 843–62. doi:10.1534/genetics.115.176503

9. Shannon KB, Li R. The multiple roles of Cyk1p in the assembly and function of the actomyosin ring in budding yeast. Mol Biol Cell. 1999;10: 283–96. doi:10.1091/mbc.10.2.283

10. Fang X, Luo J, Nishihama R, Wloka C, Dravis C, Travaglia M, et al. Biphasic targeting and cleavage furrow ingression directed by the tail of a myosin II. J Cell Biol. 2010;191: 1333–50. doi:10.1083/jcb.201005134

11. Mendes Pinto I, Rubinstein B, Kucharavy A, Unruh JR, Li R. Actin Depolymerization Drives Actomyosin Ring Contraction during Budding Yeast Cytokinesis. Dev Cell. 2012;22: 1247–60. doi:10.1016/j.devcel.2012.04.015

12. Chew TG, Huang J, Palani S, Sommese R, Kamnev A, Hatano T, et al. Actin turnover maintains actin filament homeostasis during cytokinetic ring contraction. J Cell Biol. 2017;216: 2657–2667. doi:10.1083/jcb.201701104

13. Nishihama R, Schreiter JH, Onishi M, Vallen EA, Hanna J, Moravcevic K, et al. Role of Inn1 and its interactions with Hof1 and Cyk3 in promoting cleavage furrow and septum formation in S. cerevisiae. J Cell Biol. 2009;185: 995–1012. doi:10.1083/jcb.200903125

14. Jendretzki A, Ciklic I, Rodicio R, Schmitz HP, Heinisch JJ. Cyk3 acts in

actomyosin ring independent cytokinesis by recruiting Inn1 to the yeast bud neck. Mol Genet Genomics. 2009;282: 437–51. doi:10.1007/s00438-009-0476-0

15. Wloka C, Vallen EA, Thé L, Fang X, Oh Y, Bi E. Immobile myosin-II plays a scaffolding role during cytokinesis in budding yeast. J Cell Biol. 2013;200: 271–86. doi:10.1083/jcb.201208030

16. Foltman M, Molist I, Arcones I, Sacristan C, Filali-Mouncef Y, Roncero C, et al. Ingression Progression Complexes Control Extracellular Matrix Remodelling during Cytokinesis in Budding Yeast. PLoS Genet. 2016;12: e1005864. doi:10.1371/journal.pgen.1005864

17. Foltman M, Filali-Mouncef Y, Crespo D, Sanchez-Diaz A. Cell polarity protein Spa2 coordinates Chs2 incorporation at the division site in budding yeast. PLoS Genet. 2018;14: e1007299. doi:10.1371/journal.pgen.1007299

18. Devrekanli A, Foltman M, Roncero C, Sanchez-Diaz A, Labib K. Inn1 and Cyk3 regulate chitin synthase during cytokinesis in budding yeasts. J Cell Sci. 2012;125: 5453–66. doi:10.1242/jcs.109157

19. Wang M, Nishihama R, Onishi M, Pringle JR. Role of the Hof1–Cyk3 interaction in cleavage-furrow ingression and primary-septum formation during yeast cytokinesis. Mol Biol Cell. 2018;29: 597–609. doi:10.1091/mbc.E17-04-0227

20. Sburlati A, Cabib E. Chitin synthetase 2, a presumptive participant in septum formation in Saccharomyces cerevisiae. J Biol Chem. 1986;261: 15147–52.

21. Shaw JA, Mol PC, Bowers B, Silverman SJ, Valdivieso MH, Duran A, et al. The function of chitin synthases 2 and 3 in the Saccharomyces cerevisiae cell cycle. J Cell Biol. 1991;114: 111–23. doi:10.1083/jcb.114.1.111

902 22. Wloka C, Bi E. Mechanisms of cytokinesis in budding yeast. Cytoskeleton.
903 2012;69: 710–726. doi:10.1002/cm.21046
904 23. Schmidt M, Bowers B, Varma A, Roh DH, Cabib E. In budding yeast,
905 contraction of the actomyosin ring and formation of the primary septum at
906 cytokinesis depend on each other. J Cell Sci. 2002;115: 293–302.
907 24. VerPlank L, Li R. Cell cycle-regulated trafficking of Chs2 controls actomyosin
908 ring stability during cytokinesis. Mol Biol Cell. 2005;16: 2529–43.
909 doi:10.1091/mbc.E04-12-1090
910 25. Sanchez-Diaz A, Marchesi V, Murray S, Jones R, Pereira G, Edmondson R, et
911 al. Inn1 couples contraction of the actomyosin ring to membrane ingression
912 during cytokinesis in budding yeast. Nat Cell Biol. 2008;10: 395–406.
913 doi:10.1038/ncb1701
914 26. Cabib E, Sburlati A, Bowers B, Silverman SJ. Chitin synthase 1, an auxiliary
915 enzyme for chitin synthesis in Saccharomyces cerevisiae. J Cell Biol.
916 1989;108: 1665–72. doi:10.1083/jcb.108.5.1665
917 27. Douglas CM, Foor F, Marrinan JA, Morin N, Nielsen JB, Dahl AM, et al. The
918 Saccharomyces cerevisiae FKS1 (ETG1) gene encodes an integral membrane
919 protein which is a subunit of 1,3-β-D-glucan synthase. Proc Natl Acad Sci U S
920 A. 1994;91: 12907–11. doi:10.1073/pnas.91.26.12907
921 28. Weiss EL. Mitotic exit and separation of mother and daughter cells. Genetics.
922 2012;192: 1165–1202. doi:10.1534/genetics.112.145516
923 29. Queralt E, Uhlmann F. Cdk-counteracting phosphatases unlock mitotic exit.
924 Curr Opin Cell Biol. 2008/10/11. 2008;20: 661–668. doi:S0955-
925 0674(08)00161-0 [pii] 10.1016/j.ceb.2008.09.003
926 30. Baro B, Queralt E, Monje-Casas F. Regulation of mitotic exit in saccharomyces

cerevisiae. Methods in Molecular Biology. 2017. pp. 3–17. doi:10.1007/978-1-4939-6502-1_1

31. Rock JM, Amon A. The FEAR network. Curr Biol. 2009;19: R1063-8. doi:10.1016/j.cub.2009.10.002

32. Hotz M, Barral Y. The Mitotic Exit Network: New turns on old pathways. Trends in Cell Biology. 2014. pp. 145–152. doi:10.1016/j.tcb.2013.09.010

33. Visintin R, Craig K, Hwang ES, Prinz S, Tyers M, Amon A. The Phosphatase Cdc14 Triggers Mitotic Exit by Reversal of Cdk-Dependent Phosphorylation. Mol Cell. 1998;2: 709–718. doi:10.1016/S1097-2765(00)80286-5

34. Jiménez J, Castelao BA, González-Novo A, Sánchez-Pérez M. The role of MEN (mitosis exit network) proteins in the cytokinesis of Saccharomyces cerevisiae. Int Microbiol. 2005;8: 33–42. doi:im2305005 [pii]

35. Meitinger F, Boehm ME, Hofmann A, Hub B, Zentgraf H, Lehmann WD, et al. Phosphorylation-dependent regulation of the F-BAR protein Hof1 during cytokinesis. Genes Dev. 2011/04/19. 2011;25: 875–888. doi:10.1101/gad.622411

36. Yoshida S, Kono K, Lowery DM, Bartolini S, Yaffe MB, Ohya Y, et al. Polo-like kinase Cdc5 controls the local activation of Rho1 to promote cytokinesis. Science (80- ). 2006;313: 108–111. doi:10.1126/science.1126747

37. Meitinger F, Petrova B, Lombardi IM, Bertazzi DT, Hub B, Zentgraf H, et al. Targeted localization of Inn1, Cyk3 and Chs2 by the mitotic-exit network regulates cytokinesis in budding yeast. J Cell Sci. 2010/05/06. 2010;123: 1851–1861. doi:jcs.063891 [pii] 10.1242/jcs.063891

38. Teh EM, Chai CC, Yeong FM. Retention of Chs2p in the ER requires N-terminal CDK1-phosphorylation sites. Cell Cycle. 2009;8: 2964–74.

952 39. Chin CF, Bennett AM, Ma WK, Hall MC, Yeong FM. Dependence of Chs2 ER
953 export on dephosphorylation by cytoplasmic Cdc14 ensures that septum
954 formation follows mitosis. Mol Biol Cell. 2012;23: 45–58. doi:10.1091/mbc.E11-
955 05-0434
956 40. Naylor SG, Morgan DO. Cdk1-dependent phosphorylation of iqg1 governs
957 actomyosin ring assembly prior to cytokinesis. J Cell Sci. 2014;127: 1128–37.
958 doi:10.1242/jcs.144097
959 41. Palani S, Meitinger F, Boehm ME, Lehmann WD, Pereira G. Cdc14-dependent
960 dephosphorylation of Inn1 contributes to Inn1-Cyk3 complex formation. J Cell
961 Sci. 2012/03/29. 2012;125: 3091–3096. doi:10.1242/jcs.106021
962 42. Kuilman T, Maiolica A, Godfrey M, Scheidel N, Aebersold R, Uhlmann F.
963 Identification of Cdk targets that control cytokinesis. EMBO J. 2015;34: 81–96.
964 doi:10.15252/embj.201488958
965 43. Miller DP, Hall H, Chaparian R, Mara M, Mueller A, Hall MC, et al.
966 Dephosphorylation of Iqg1 by Cdc14 regulates cytokinesis in budding yeast.
967 Mol Biol Cell. 2015;26: 2913–26. doi:10.1091/mbc.E14-12-1637
968 44. Sanchez-Diaz A, Nkosi PJ, Murray S, Labib K, Sanchez-Diaz A, Nkosi PJ, et
969 al. The Mitotic Exit Network and Cdc14 phosphatase initiate cytokinesis by
970 counteracting CDK phosphorylations and blocking polarised growth. EMBO J.
971 2012;31: 3620–3634. doi:10.1038/emboj.2012.224
972 45. Touati SA, Hofbauer L, Jones AW, Snijders AP, Kelly G, Uhlmann F. Cdc14
973 and PP2A Phosphatases Cooperate to Shape Phosphoproteome Dynamics
974 during Mitotic Exit. Cell Rep. 2019;29: 2015–2119.
975 doi:10.1016/j.celrep.2019.10.041
976 46. Touati SA, Kataria M, Jones AW, Snijders AP, Uhlmann F. Phosphoproteome

977 dynamics during mitotic exit in budding yeast. EMBO J. 2018;37: e98745.
978 doi:10.15252/embj.201798745
979 47. Healy AM, Zolnierowicz S, Stapleton AE, Goebl M, DePaoli-Roach AA, Pringle
980 JR. CDC55, a Saccharomyces cerevisiae gene involved in cellular
981 morphogenesis: identification, characterization, and homology to the B subunit
982 of mammalian type 2A protein phosphatase. Mol Cell Biol. 1991;11: 5767–
983 5780. doi:10.1128/mcb.11.11.5767
984 48. Shu Y, Yang H, Hallberg E, Hallberg R. Molecular genetic analysis of Rts1p, a
985 B' regulatory subunit of Saccharomyces cerevisiae protein phosphatase 2A.
986 Mol Cell Biol. 1997;17: 3242–3253. doi:10.1128/mcb.17.6.3242
987 49. Jiang Y, Broach JR. Tor proteins and protein phosphatase 2A reciprocally
988 regulate Tap42 in controlling cell growth in yeast. EMBO J. 1999;18: 2782–92.
989 doi:10.1093/emboj/18.10.2782
990 50. Jonasson EM, Rossio V, Hatakeyama R, Abe M, Ohya Y, Yoshida S.
991 Zds1/Zds2–PP2A(Cdc55) complex specifies signaling output from Rho1
992 GTPase. J Cell Biol. 2016;212: 51–61. doi:10.1083/jcb.201508119
993 51. Yaakov G, Thorn K, Morgan DO. Separase Biosensor Reveals that Cohesin
994 Cleavage Timing Depends on Phosphatase PP2ACdc55 Regulation. Dev Cell.
995 2012;23: 124–136. doi:10.1016/j.devcel.2012.06.007
996 52. Pal G, Paraz MT, Kellogg DR. Regulation of Mih1/Cdc25 by protein
997 phosphatase 2A and casein kinase 1. J Cell Biol. 2008/03/05. 2008;180: 931–
998 945. doi:jcb.200711014 [pii] 10.1083/jcb.200711014
999 53. Juanes MA, Khoueiry R, Kupka T, Castro A, Mudrak I, Ogris E, et al. Budding
1000 Yeast Greatwall and Endosulfines Control Activity and Spatial Regulation of
1001 PP2ACdc55 for Timely Mitotic Progression. PLoS Genet. 2013;9: e1003575.

1002 doi:10.1371/journal.pgen.1003575

1003 54. Vernieri C, Chiroli E, Francia V, Gross F, Ciliberto A. Adaptation to the spindle
1004 checkpoint is regulated by the interplay between Cdc28/Clbs and PP2ACdc55.
1005 J Cell Biol. 2013;202: 765–778. doi:10.1083/jcb.201303033

1006 55. Queralt E, Uhlmann F. Separase cooperates with Zds1 and Zds2 to activate
1007 Cdc14 phosphatase in early anaphase. J Cell Biol. 2008;182: 873–883.
1008 doi:10.1083/jcb.200801054

1009 56. Queralt E, Lehane C, Novak B, Uhlmann F. Downregulation of PP2ACdc55
1010 Phosphatase by Separase Initiates Mitotic Exit in Budding Yeast. Cell.
1011 2006;125: 719–732. doi:10.1016/j.cell.2006.03.038

1012 57. Baro B, Rodriguez-Rodriguez J-A, Calabria I, Hernáez ML, Gil C, Queralt E.
1013 Dual Regulation of the Mitotic Exit Network (MEN) by PP2A-Cdc55
1014 Phosphatase. PLoS Genet. 2013;9: e1003966.
1015 doi:10.1371/journal.pgen.1003966

1016 58. Baro B, Játiva S, Calabria I, Vinaixa J, Bech-Serra JJ, De LaTorre C, et al.
1017 SILAC-based phosphoproteomics reveals new PP2A-Cdc55-regulated
1018 processes in budding yeast. Gigascience. 2018;7: giy407.
1019 doi:10.1093/gigascience/giy047

1020 59. Korinek WS, Bi E, Epp JA, Wang L, Ho J, Chant J. Cyk3, a novel SH3-domain
1021 protein, affects cytokinesis in yeast. Curr Biol. 2000;10: 947–50.
1022 doi:10.1016/S0960-9822(00)00626-6

1023 60. Nishimura K, Fukagawa T, Takisawa H, Kakimoto T, Kanemaki M. An auxin-
1024 based degron system for the rapid depletion of proteins in nonplant cells. Nat
1025 Methods. 2009;6: 917–22. doi:10.1038/nmeth.1401

1026 61. Vallen EA, Caviston J, Bi E. Roles of Hof1p, Bni1p, Bnr1p, and Myo1p in

cytokinesis in Saccharomyces cerevisiae. Mol Biol Cell. 2000;11: 593–611. doi:10.1091/mbc.11.2.593

62. Jakobsen MK, Cheng Z, Lam SK, Roth-Johnson E, Barfield RM, Schekman R. Phosphorylation of Chs2p regulates interaction with COPII. J Cell Sci. 2013;126: 2151–6. doi:10.1242/jcs.115915

63. Oh Y, Chang KJ, Orlean P, Wloka C, Deshaies R, Bi E. Mitotic exit kinase Dbf2 directly phosphorylates chitin synthase Chs2 to regulate cytokinesis in budding yeast. Mol Biol Cell. 2012/05/11. 2012;23: 2445–2456. doi:mbc.E12-01-0033 [pii] 10.1091/mbc.E12-01-0033

64. Játiva S, Calabria I, Moyano-Rodriguez Y, Garcia P, Queralt E. Cdc14 activation requires coordinated Cdk1-dependent phosphorylation of Net1 and PP2A–Cdc55 at anaphase onset. Cell Mol Life Sci. 2019;76: 3601–3620. doi:10.1007/s00018-019-03086-5

65. Kim HB, Haarer BK, Pringle JR. Cellular morphogenesis in the Saccharomyces cerevisiae cell cycle: localization of the CDC3 gene product and the timing of events at the budding site. J Cell Biol. 1991;112: 535–544. doi:10.1083/jcb.112.4.535

66. Iwase M, Luo J, Nagaraj S, Longtine M, Kim HB, Haarer BK, et al. Role of a Cdc42p effector pathway in recruitment of the yeast septins to the presumptive bud site. Mol Biol Cell. 2006;17: 1110–25. doi:10.1091/mbc.E05-08-0793

67. Lippincott J, Li R. Sequential assembly of myosin II, an IQGAP-like protein, and filamentous actin to a ring structure involved in budding yeast cytokinesis. J Cell Biol. 1998;140: 355–66. doi:10.1083/jcb.140.2.355

68. McQuilken M, Jentzsch MS, Verma A, Mehta SB, Oldenbourg R, Gladfelter AS. Analysis of septin reorganization at cytokinesis using polarized

fluorescence microscopy. Front Cell Dev Biol. 2017;5: 42. doi:10.3389/fcell.2017.00042

69. Tamborrini D, Juanes MA, Ibanes S, Rancati G, Piatti S. Recruitment of the mitotic exit network to yeast centrosomes couples septin displacement to actomyosin constriction. Nat Commun. 2018;9: 4308. doi:10.1038/s41467-018-06767-0

70. Lew DJ, Reed SI. Morphogenesis in the yeast cell cycle: Regulation by Cdc28 and cyclins. J Cell Biol. 1993;120: 1305–1320. doi:10.1083/jcb.120.6.1305

71. Kennedy EK, Dysart M, Lianga N, Williams EC, Pilon S, Doré C, et al. Redundant regulation of Cdk1 tyrosine dephosphorylation in Saccharomyces cerevisiae. Genetics. 2016;202: 903–10. doi:10.1534/genetics.115.182469

72. Minshull J, Straight A, Rudner AD, Dernburg AF, Belmont A, Murray AW. Protein phosphatase 2A regulates MPF activity and sister chromatid cohesion in budding yeast. Curr Biol. 1996;6: 1609–1620. doi:10.1016/S0960-9822(02)70784-7

73. Cabib E, Schmidt M. Chitin synthase III activity, but not the chitin ring, is required for remedial septa formation in budding yeast. FEMS Microbiol Lett. 2003;224: 299–305. doi:10.1016/S0378-1097(03)00477-4

74. Holt LJ, Tuch BB, Villén J, Johnson AD, Gygi SP, Morgan DO, et al. Global analysis of Cdk1 substrate phosphorylation sites provides insights into evolution. Science. 2009;325: 1682–6. doi:10.1126/science.1172867

75. Chin CF, Tan K, Onishi M, Chew YY, Augustine B, Lee WR, et al. Timely Endocytosis of Cytokinetic Enzymes Prevents Premature Spindle Breakage during Mitotic Exit. PLoS Genet. 2016;12: e1006195. doi:10.1371/journal.pgen.1006195

1077 76. Dobbelaere J, Gentry MS, Hallberg RL, Barral Y. Phosphorylation-dependent
1078 regulation of septin dynamics during the cell cycle. Dev Cell. 2003;4: 345–57.
1079 doi:10.1016/S1534-5807(03)00061-3
1080 77. Gentry MS, Hallberg RL. Localization of Saccharomyces cerevisiae protein
1081 phosphatase 2A subunits throughout mitotic cell cycle. Mol Biol Cell. 2002;13:
1082 3477–3492. doi:10.1091/mbc.02-05-0065
1083 78. Park SY, Cable AE, Blair J, Stockstill KE, Shannnon KB. Bub2 regulation of
1084 cytokinesis and septation in budding yeast. BMC Cell Biol. 2009;10: 43.
1085 doi:10.1186/1471-2121-10-43
1086 79. Oh Y, Schreiter JH, Okada H, Wloka C, Okada S, Yan D, et al. Hof1 and Chs4
1087 Interact via F-BAR Domain and Sel1-like Repeats to Control Extracellular
1088 Matrix Deposition during Cytokinesis. Curr Biol. 2017;27: 2878–2886.
1089 doi:10.1016/j.cub.2017.08.032
1090 80. Godfrey M, Touati SA, Kataria M, Jones A, Snijders AP, Uhlmann F.
1091 PP2A(Cdc55) Phosphatase Imposes Ordered Cell-Cycle Phosphorylation by
1092 Opposing Threonine Phosphorylation. Mol Cell. 2017;65: 393-402.e3.
1093 doi:10.1016/j.molcel.2016.12.018
1094 81. Knop M, Siegers K, Pereira G, Zachariae W, Winsor B, Nasmyth K, et al.
1095 Epitope tagging of yeast genes using a PCR-based strategy: More tags and
1096 improved practical routines. Yeast. 1999;15: 963–972. doi:10.1002/(SICI)1097-
1097 0061(199907)15:10B<963::AID-YEA399>3.0.CO;2-W
1098 82. Monje-Casas F, Queralt E. The Mitotic Exit Network. Fernando Monje-Casas
1099 EQ, editor. Humana Press; 2017. doi:10.1007/978-1-4939-6502-1
1100 83. Schindelin J, Arganda-Carreras I, Frise E, Kaynig V, Longair M, Pietzsch T, et
1101 al. Fiji: An open-source platform for biological-image analysis. Nat Methods.

2012;9: 676–82. doi:10.1038/nmeth.2019

## Figure legends

**Figure 1. PP2A$^{Cdc55}$ participates in the dephosphorylation of IPC proteins during anaphase and cytokinesis.** (a) The double mutants *cdc55 hof1* and *cdc55 cyk3* are synthetic sick. Serial dilutions of W303, Y844, Y1728, Y1730, Y1747, and Y1749 were spotted in YPD plates, with and without 1.5 mM auxin (IAA). Cells were grown at 25ºC for 2-3 days. (b-e) PP2A$^{Cdc55}$ regulates Hof1 and Inn1 dephosphorylation. Strains Y1314, Y1394, Y1639, Y1640, Y1437, Y1438, Y1318 and Y1315 were arrested in metaphase and released into anaphase by Cdc20 depletion and re-addition. Proteins phosphorylations were analyzed by western blot in Phos-tag gels. Unspecific bands were detected for Chs2 and marked as (ª). Pgk1 levels were used as a loading control. Mitosis progression was followed by analyzing the anaphase spindle elongation by *in situ* immunofluorescence. At least 100 cells were scored at each time-point. Quantification of the western blots was perform using Fiji Software and means and SEMs are represented. Student's unpaired t-test analyses were carried out using the Prism5 program. (f) PP2A$^{Cdc55}$ forms a complex with IPC proteins. Strains Y1565, Y1566, Y1423, and Y1567 were synchronized into anaphase progression by Cdc20 depletion and re-addition. Strains Y1437, Y1312, Y1314, and Y1318 without Pk-Cdc55 were used as negative controls. Protein extracts were prepared at metaphase, anaphase, and cytokinesis. Cdc55 was purified by immunoprecipitation with Pk antibody. Co-purification of Cyk3-HA$_6$, Inn1-HA$_6$, Hof1-HA$_6$, and Chs2-HA$_6$ was analyzed by western blot.

**Figure 2. PP2A$^{Cdc55}$ dephosphorylates Hof1 and Chs2 *in vitro*.** Strains Y824, Y1652 and Y1653 were arrested in metaphase by Cdc20 depletion. Cdc55 and *cdc55-ED* were purified by immunoprecipitation with HA antibody. $^{32}$P-Hof1 obtained from the Clb2-Cdk1 kinase assays (a), and $^{32}$P-Chs2 phosphorylated by Cdk1-Clb2 (b) or Dbf2-Mob1 (c) were used as substrate in the phosphatase assays. Representative images of the phosphatase assays are shown. Quantification of the remaining phosphorylation signals normalized with respect to the amount of immunopurified HA-Cdc55 or HA-*cdc55-ED* are shown. Means and SEMs of three phosphatase assays are represented. Student's paired t-test analysis was carried out using the Prism5 program.

**Figure 3. PP2A$^{Cdc55}$ regulates AMR constriction and septum formation.** (a) Absence of Cdc55 promotes the asymmetry of Myo1-tdTomato signal upon AMR contraction. Strains Y1306 and Y1578 were arrested in metaphase and released into anaphase by Cdc20 depletion and re-addition, and time-lapse images were captured every 2 minutes. Spc42-GFP (spindle pole body protein) was used as the control for anaphase progression. Maximum intensity z-projection images of Myo1-tdTomato signal in *CDC55* and *cdc55Δ* are shown (left panel). Quantification of the contraction time of Myo1-tdTomato (right panel). (b) Quantification of the population of cells with asymmetric Myo1 constriction in *CDC55* (N=30) and *cdc55Δ* (N=30) from (a) is shown. (c) PP2A$^{Cdc55\text{-}ED}$ inactive phosphatase promotes Myo1 asymmetry in a similar way to the *cdc55Δ* deletion mutant. Strains Y1652, Y1653 and Y1788 were arrested in metaphase and released into anaphase by Cdc20 depletion and re-addition. *cdc55-aid* degradation was induced by the addition of 0.5 mM auxin for 3 hours during the metaphase arrest and auxin was maintained after Cdc20 re-addition.

Time-lapse images were captured every 2 minutes. Quantification of the cell population with asymmetric Myo1 constriction in Cdc55 (N=9), *cdc55-aid* (N=35) and *cdc55-ED* (N=17) is shown (left panel). Maximum intensity z-projection images of Myo1-tdTomato signal from Cdc55, *cdc55-aid* and *cdc55-ED* cells (right panel). Scale bar, 1 μm. (d) Chitin deposition at primary and secondary septa is regulated by $PP2A^{Cdc55}$**.** Strains Y1516, Y1512, Y1605, and Y1596 were arrested in metaphase by Cdc20 depletion, and released into anaphase by Cdc20 re-induction. 50 μg calcofluor was added to visualize both septa (left panel) and primary septum (right panel). Scale bar, 2 μm. Student's unpaired t-test was carried out using the Prism5 program

**Figure 4. Asymmetric primary septum formation and appearance of the remedial septum in the absence of Cdc55.** Strains Y1315 (WT), Y1318 (*cdc55Δ*), Y1605 (*chs3Δ*), and Y1596 (*cdc55Δ chs3Δ*) were arrested in metaphase and released into anaphase by Cdc20 depletion and re-addition. Representative images from TEM are shown. Scale bar, 0.5 μm. PS, SS and RS denotes primary septum, secondary septa and remedial septum respectively.

**Figure 5. $PP2A^{Cdc55}$ is required for proper IPC localization and contraction at the division site.** Strains Y1576, Y1575, Y1574, Y1604, Y1306, Y1578, Y1454, Y1608, Y1572, and Y1606 were synchronized into anaphase by Cdc20 depletion and re-addition, and time-lapse images were captured every 2 minutes. Spc42-GFP and Myo1-tdTomato were used as a control for cytokinesis progression. (a) Percentage of cells with IPC asymmetric signal is shown (left panel). Maximum intensity z-projection images of Chs2-GFP, Cyk3-GFP, Hof1-GFP, Inn1-GFP and

Iqg1-GFP signal in *CDC5*5 and cdc55*Δ* are shown (right panel). (b) Quantification of the Iqg1-GFP and Hof1-GFP signal from the onset of contraction until the signal disappearance relative to the Myo1 signal contraction. (c) Analysis of the time of localization at the division site of Cyk3-GFP, Inn1-GFP, and Chs2-GFP. Student's unpaired t-test was carried out using the Prism5 program.

**Figure 6. The non-phosphorylable *chs2-6A* version rescues the asymmetric AMR contraction in the *cdc55Δ* mutant cells.** Strains Y1852 containing control *GAL1-CHS2* and Y1830 the non-phosphorylable *GAL1-chs2-6A* mutant in a *cdc55Δ* mutant were arrested at metaphase by Cdc20 depletion. Galactose was added for 3 hours before synchronous release into anaphase by Cdc20 re-introduction and time-lapse images were captured every 2 minutes to visualize Myo1-tdTomato and Chs2-YFP. (a) Percentage of cells with asymmetric Myo1 and Chs2 signal is represented. Representative images of Myo1 and Chs2 are shown. (b) Quantifications of the contraction time of Myo1-tdTomato and Chs2-YFP are depicted.

**Figure 7. Model for PP2A$^{Cdc55}$ regulation of actomyosin ring (AMR) contraction, primary septum (PS) and secondary septa (SS) formation**. Dephosphorylation of Hof1 and Chs2 by PP2A$^{Cdc55}$ coordinates AMR contraction and primary septum formation. Increased Hof1 residence time at the division site delays formation of secondary septa.

**Supplemental Figure legends**

**Figure S1. PP2A$^{Cdc55}$ regulates Iqg1 phosphorylation, but not Myo1.** (a) Strains Y1491 and Y1497 were arrested in metaphase by Cdc20 depletion and released into anaphase by Cdc20 re-addition. Myo1 and Iqg1 phosphorylation were analyzed by western blot in Phos-tag gels. Myo1-Flag levels were used as the loading control. Mitosis progression was followed by FACS analysis of DNA content and anaphase spindle elongation by *in situ* immunofluorescence. At least 100 cells were scored at each time point. Means and SEMs are represented (bottom). Student's unpaired t-test analysis was carried out using the Prism5 software. (b) Alkaline phosphatase assay for Chs2. Native protein extracts were prepared from Y1318 arrested in metaphase. PhosStop was used as the alkaline phosphatase's inhibitor. Protein phosphorylation was analyzed by western blot in Phos-tag gels.

**Figure S2. Inn1, Hof1, and Chs2 *in vitro* phosphorylation by mitotic kinases.** Strains Y824, Y688, Y2231, and Y1357 were arrested in metaphase by Cdc20 depletion. Strain Y1357 was released into anaphase by Cdc20 re-addition and samples were collected at 30 min when cells were in anaphase. Protein kinases were purified by immunoprecipitation with Pk antibody. $_{6}$His-Inn1, $_{6}$His-Hof1 and Strep-tag-Chs2-1-629 purified from *E. coli* were used as substrates. (a) Inn1 was phosphorylated by Clb2-Cdk1; (b) Hof1 was phosphorylated by Clb2-Cdk1; and (c) Chs2 was phosphorylated by Clb2-Cdc28 and Dbf2. Representative western blots of the kinase assays are shown. The quantity of kinases immunoprecipitated was analyzed by western blot. Radioactive signals were detected using a multi-purpose imaging plate (GE healthcare) in a Typhoon FLA950 apparatus. Protein levels were quantified using Fiji software.

**Figure S3. Septin structures are not altered in the absence of Cdc55.** Cycling cells from strains Y1588 and Y1589 were fixed and immunofluorescence *in situ* performed for septins Cdc11 and Shs1-HA visualization. α-Cdc11 and α-HA clone 12CA5 antibodies were used. Representative images of Cdc11 and Shs1-HA septin structures from *CDC55* and *cdc55Δ* cells are shown. Scale bar, 1 μm.

**Figure S4. Actin is polarized to the new bud site before cytokinesis completion in *cdc55Δ* cells.** Strains Y1434 (*CDC55*) and Y1435 (*cdc55Δ*) were arrested in metaphase by Cdc20 depletion and released into anaphase by Cdc20 re-induction. Formaldehyde-fixed cells were stained with 50 U/mL of rhodamine phalloidin. (a) Maximum intensity z-projection images of the actin staining and Myo1-GFP signals from *CDC55* and *cdc55Δ* at different cell cycle stages (metaphase, anaphase, cytokinesis and the next S phase are shown. (b) Quantification and representative images of the cells with re-polarized actin at the new bud site are shown. Scale bar, 1 μm.

**Figure S5. Myo1 asymmetric signal in *cdc55Δ* cells is not a consequence of its tagging or the synchronization method used.** Strains Y1434 and Y1435 were arrested in metaphase and released into anaphase by Cdc20 depletion and re-addition. Strains Y1725 and Y1761 were arrested in G1 by α-factor addition and released into cell cycle progression by pheromone removal. Cells were fixed with formaldehyde before taking images. Quantification of the cell population with asymmetric Myo1 signal is shown (upper panel). Representative images of the

Myo1-GFP signal from *CDC55* and *cdc55Δ* cells, and Myo1-tdTomato from *CDC55* *cdc28-Y19F* cells are shown (lower panel). Scale bar, 1 μm.

**Figure S6. Proper cytoplasm separation during membrane abscission in the absence of Cdc55.** Strains Y1717 and Y1708 were arrested in metaphase by Cdc20 depletion and released into anaphase by Cdc20 re-induction. Time-lapse images were captured every 2 minutes. Membrane abscission was followed by 3GFP-Ras2 signal, and Myo1-tdTomato was used as a control for cytokinesis progression. Representative images from *CDC55* (N=12) and *cdc55Δ* (N=13) cells are shown. Images are taken from the best z-stack to visualize the division site. Scale bar, 1 μm. Cumulative percentage of cells abscised is represented (lower panel).

**Figure S7. IPCs localization at the division site**. All strains were synchronized at the metaphase to anaphase transition by Cdc20 depletion and re-addition. Time-lapse images were captured every 2 minutes. Spc42-GFP and Myo1-tdTomato were used as a control for cytokinesis progression. Maximum intensity z-projection images of IPCs GFP-tagged proteins and Myo1-tdTomato contraction signals from *CDC55* and *cdc55Δ* cells are shown. (a) Iqg1 contraction at the bud neck is normal in the absence of Cdc55. Strains Y1572 and Y1606 were used. (b) Hof1 contraction is longer in the absence of Cdc55. Strains Y1306 and Y1578 were used. (c) Cyk3-GFP residence time in the bud neck is longer in *cdc55Δ* cells. Strains Y1574 and Y1604 were used. (d) Inn1-GFP residence time in the bud neck is not dependent on the presence of Cdc55. Strains Y1454 and Y1608 were used. (e)

1275 Chs2-GFP residence time in the bud neck is affected by Cdc55. Strains Y1576 and

1276 Y1575 were used. Scale bar, 1 μm.

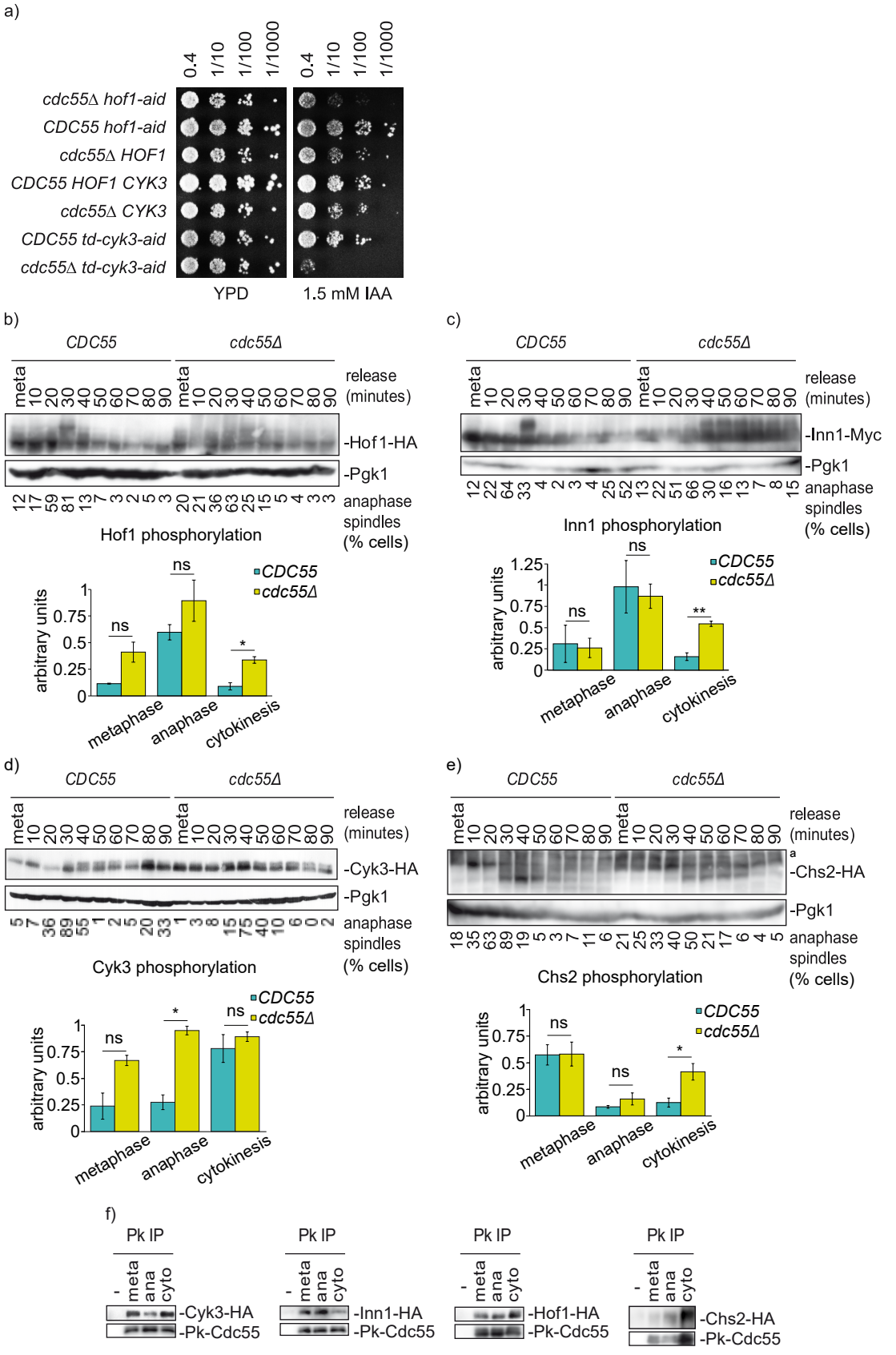

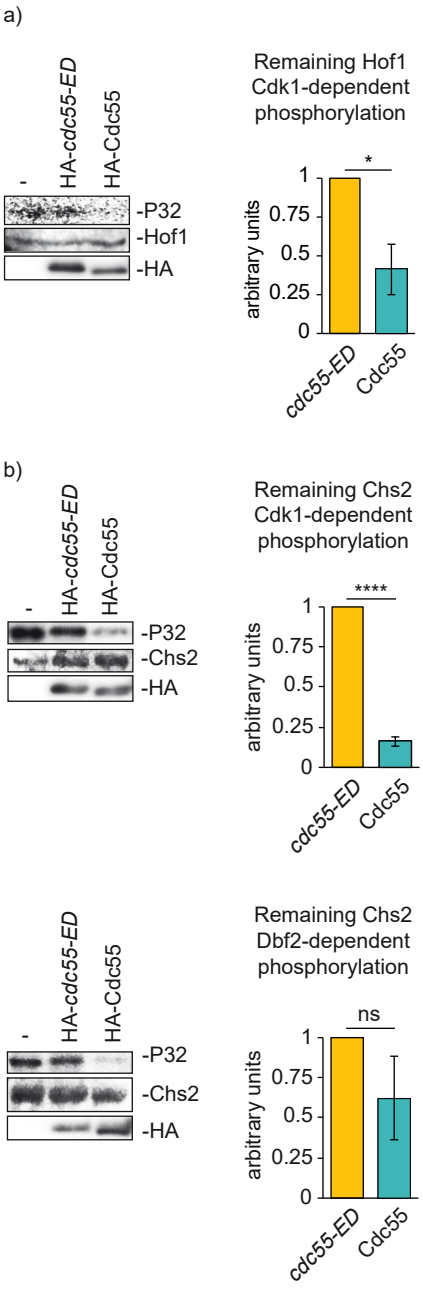

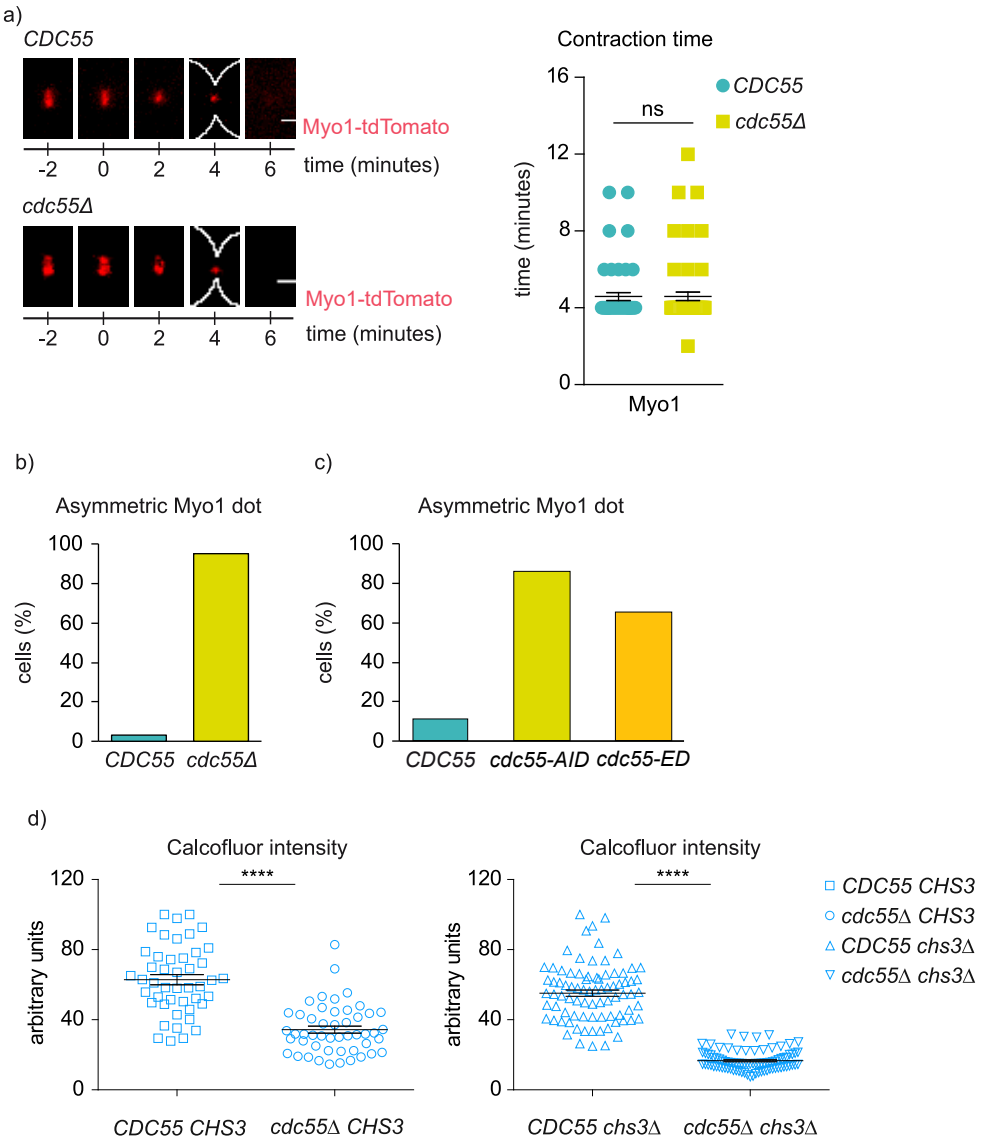

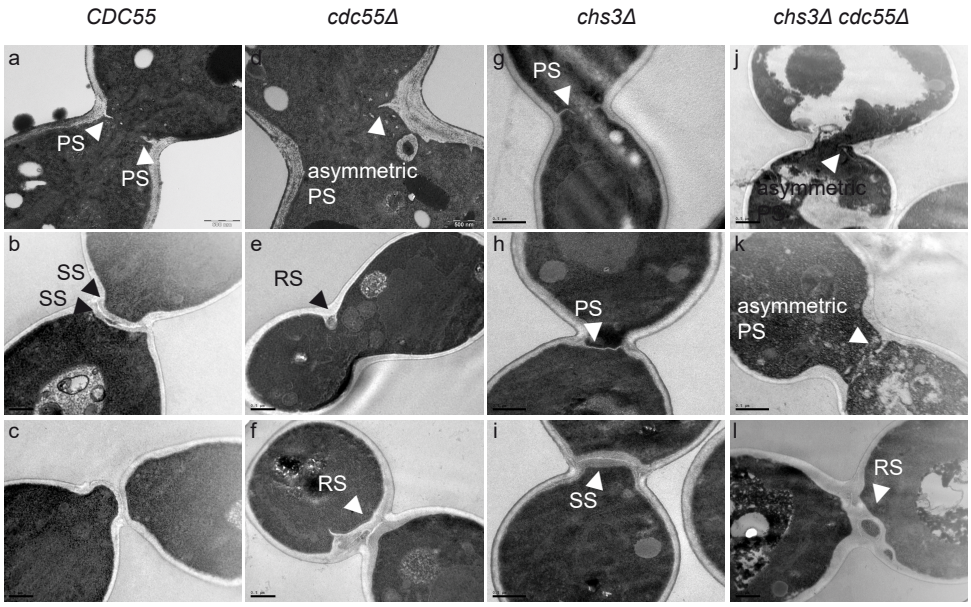

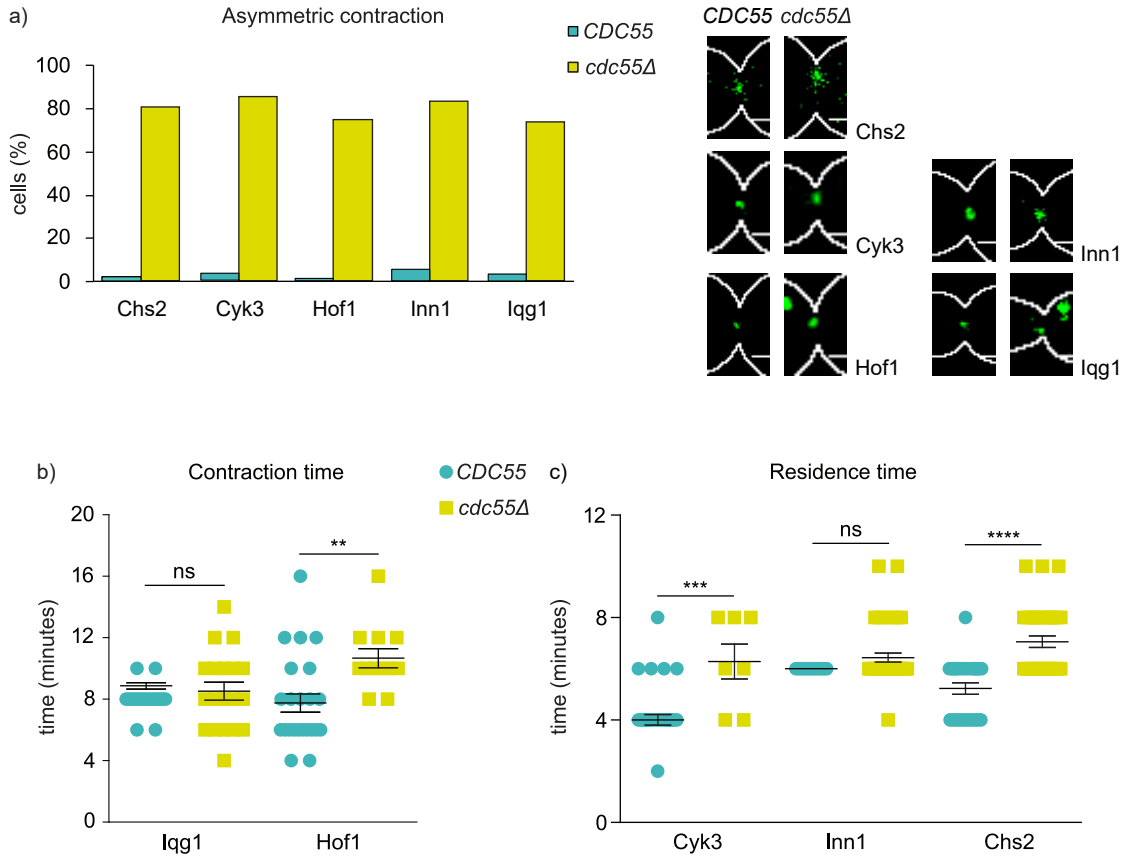

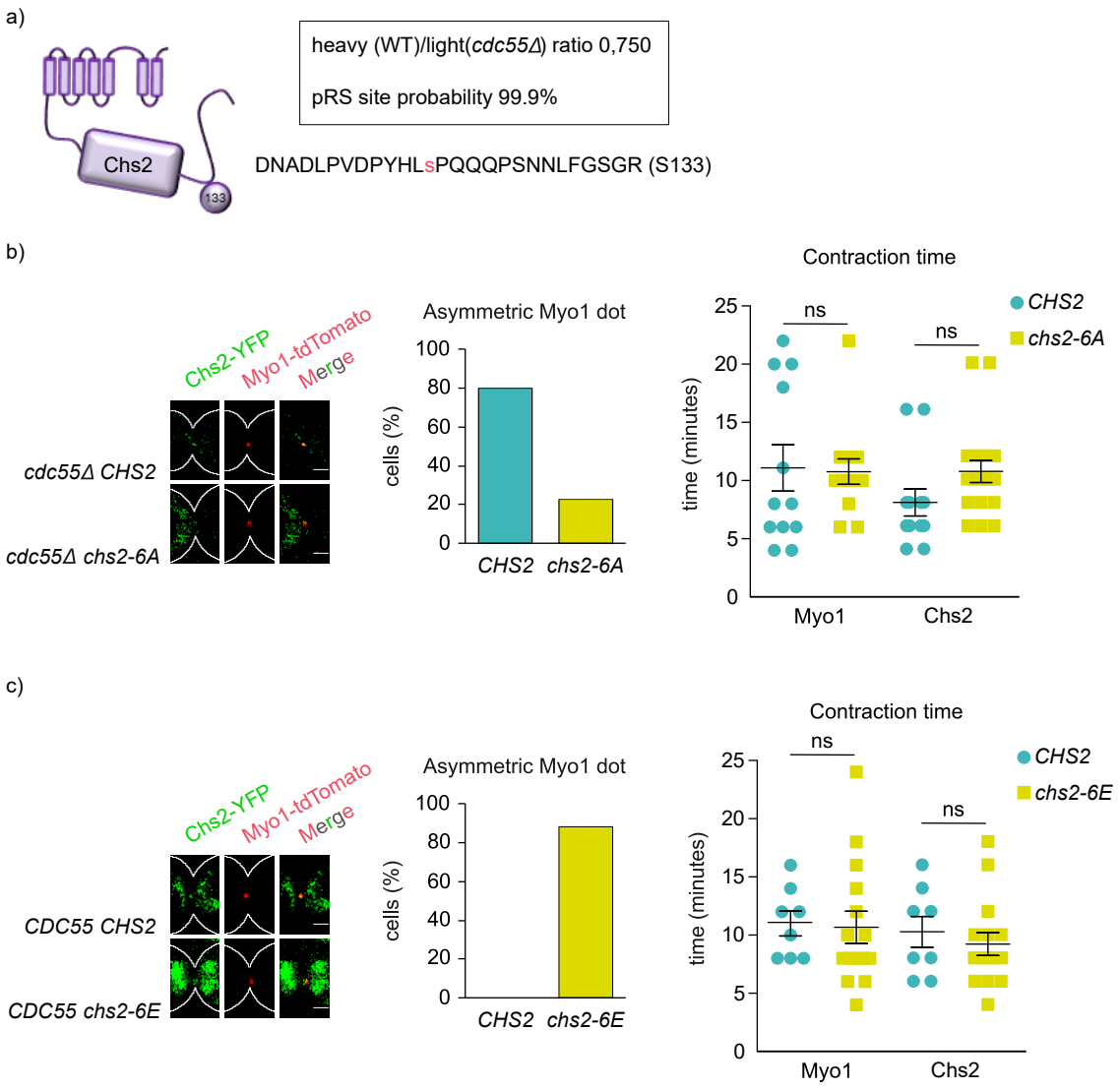

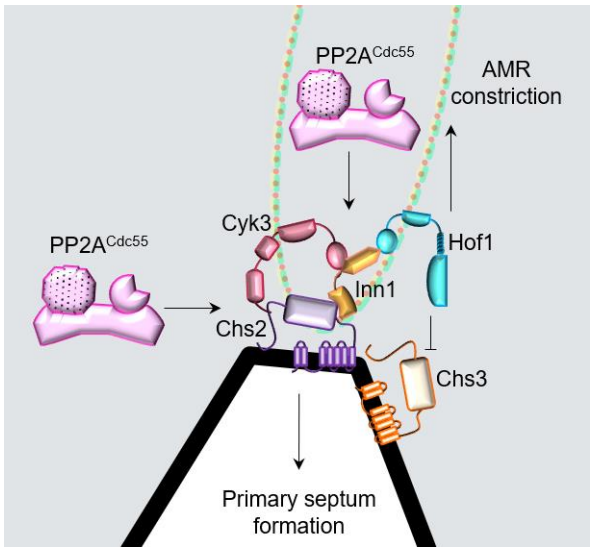
PP2A^Cdc55
AMR
constriction
Cyk3
PP2A^Cdc55
Hof1
Inn1
Chs2
Chs3
Primary septum
formation

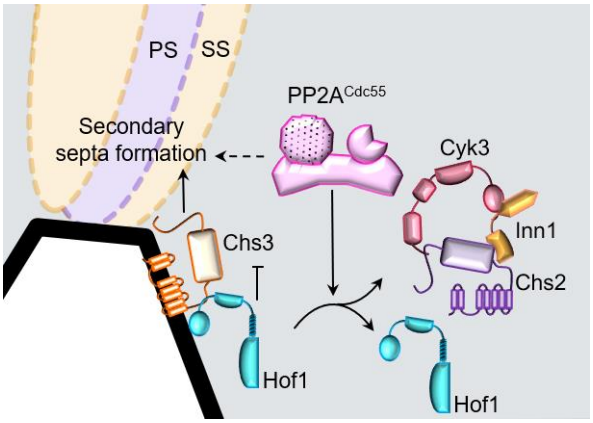
PS
SS
PP2A^Cdc55
Secondary
septa formation
Cyk3
Inn1
Chs3
Chs2
Hof1
Hof1

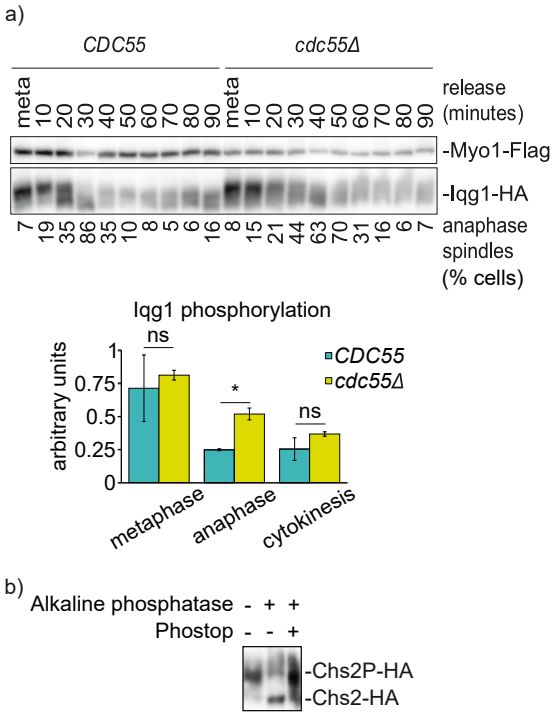
a)
CDC55
cdc55Δ
meta 10 20 30 40 50 60 70 80 90
meta 10 20 30 40 50 60 70 80 90
release (minutes)
-Myo1-Flag
-Iqg1-HA
7 19 35 86 35 10 8 5 6 16
8 15 21 44 63 70 31 16 6 7
anaphase spindles (% cells)
Iqg1 phosphorylation
arbitrary units
1
0.75
0.5
0.25
0
ns
*
ns
CDC55
cdc55Δ
metaphase
anaphase
cytokinesis
b)
Alkaline phosphatase - + +
Phostop - - +
-Chs2P-HA
-Chs2-HA

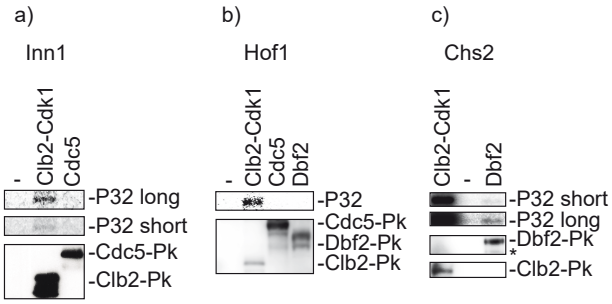

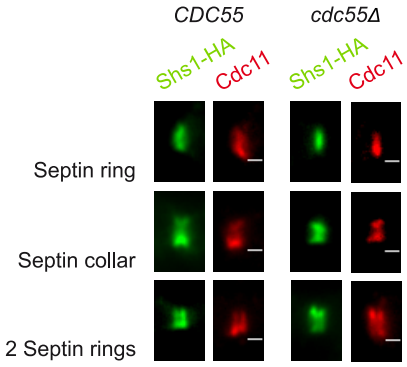

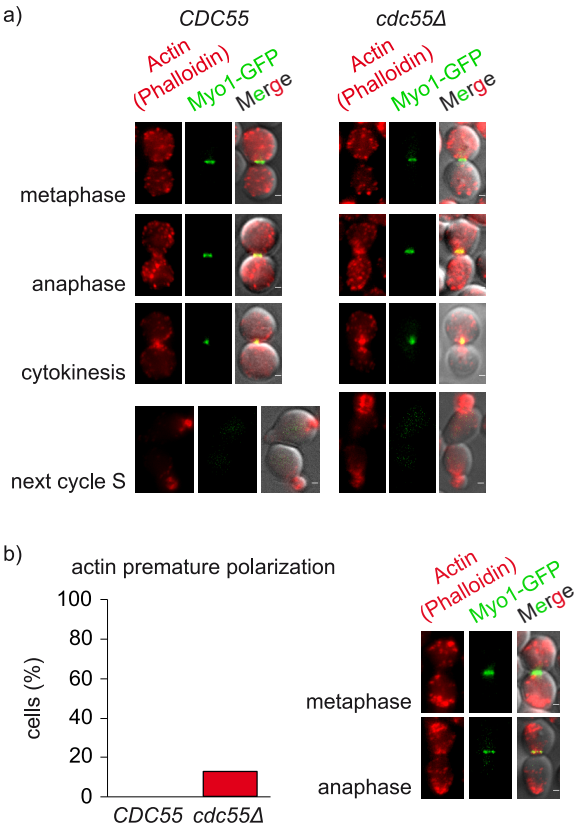

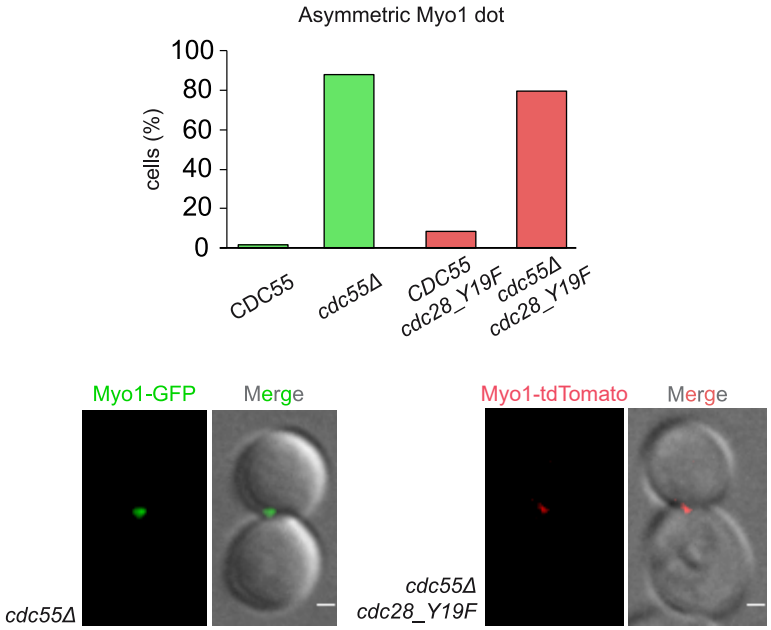

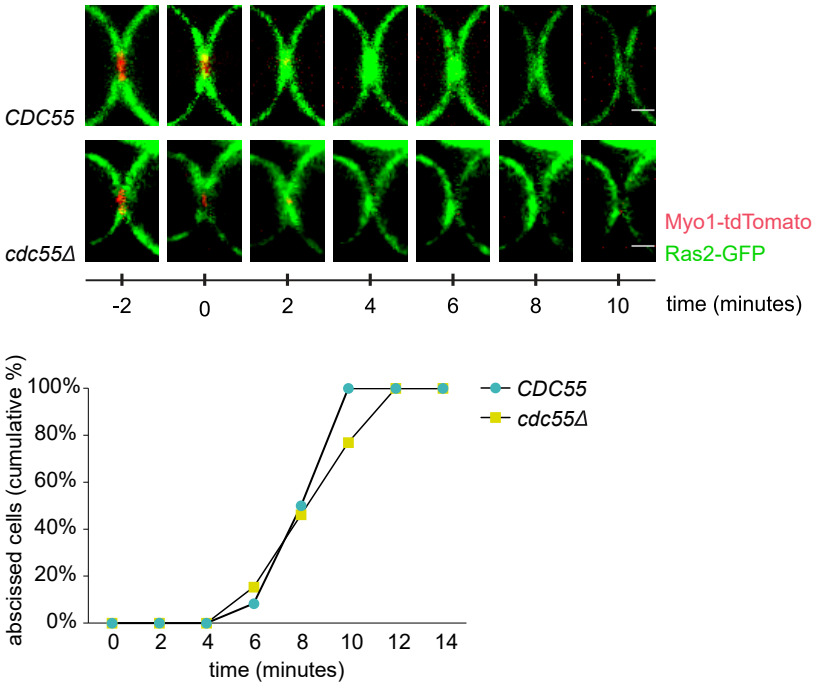

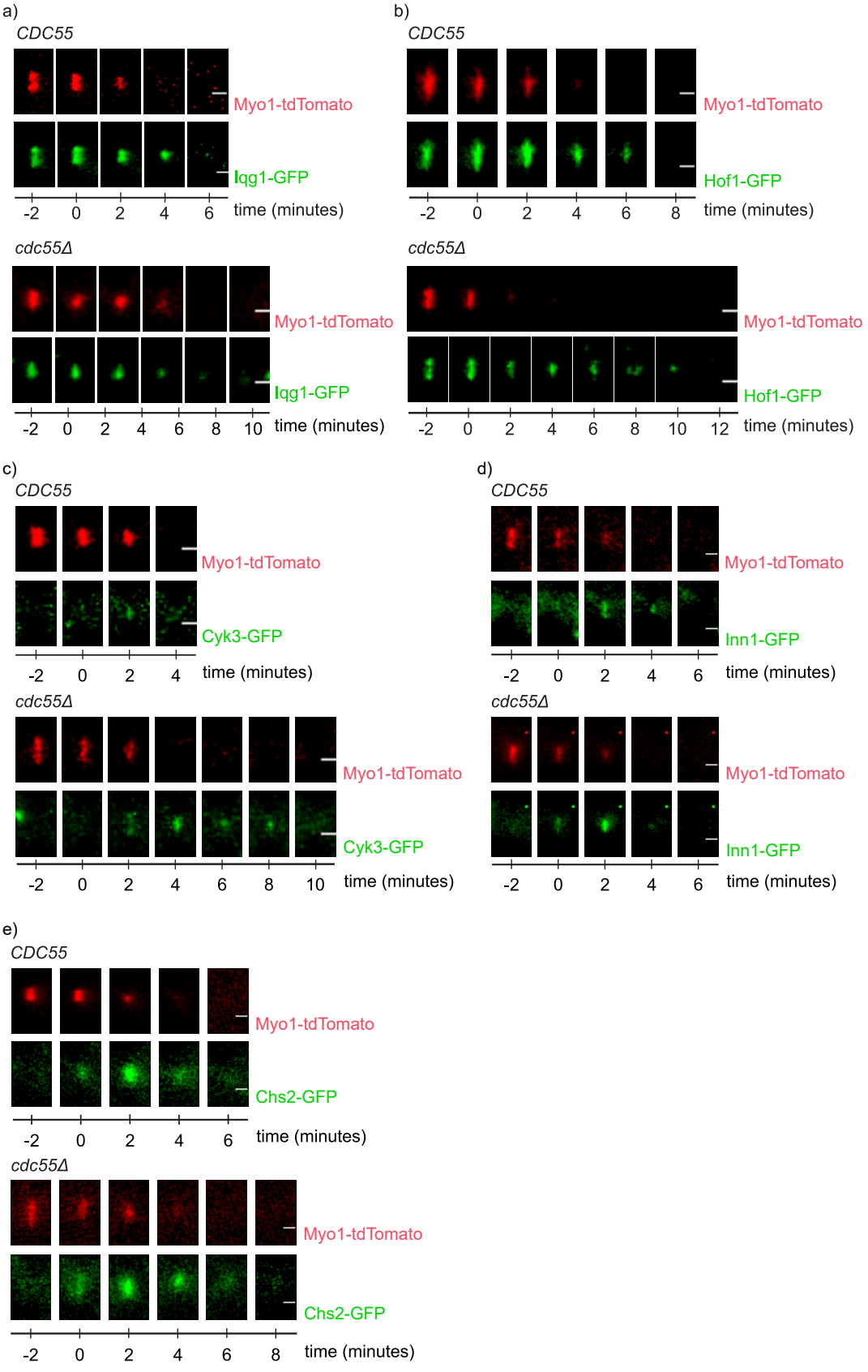

Table S1. List of strains used in this study

| Strain | Genotype | Origin |
|---|---|---|
| W303 | *MATa ade2-1 trp1-1 can1-100 leu2-3,112 his3-11,15 ura3 GAL psi+* | Matt Sullivan |
| Y688 | *MATa MET-HA3-CDC20 GAL1-FLAG-ESP1-CBD-C1531A CLB2-PK3 BFA1-HA6* | This laboratory |
| Y824 | *MATα MET-HA3-CDC20* | This laboratory |
| Y844 | *MATα cdc55Δ* | This laboratory |
| Y1306 | *MATα MET-HA3-CDC20 MYO1-TOMATOE SPC42-GFP HOF1-GFP* | This study |
| Y1312 | *MATa MET-HA3-CDC20 INN1-HA6 cdc55Δ* | This study |
| Y1314 | *MATa MET-HA3-CDC20 HOF1-HA6* | This study |
| Y1315 | *MATα MET-HA3-CDC20 CHS2-HA6 cdc55Δ* | This study |
| Y1318 | *MATa MET-HA3-CDC20 CHS2-HA6* | This study |
| Y1357 | *MATa MET-HA3-CDC20 cdc5-as NET1-MYC9 CDC5 (5´UTR):CDC5-MYC9 DBF2-PK6* | This study |
| Y1394 | *MATα MET-HA3-CDC20 HOF1-HA6 cdc55Δ* | This study |
| Y1423 | *MATa MET-HA3-CDC20 HOF1-HA6 PK3-CDC55* | This study |
| Y1434 | *MATa MET-HA3-CDC20 MYO1-GFP cdc55Δ* | This study |
| Y1435 | *MATa MET-HA3-CDC20 MYO1-GFP* | This study |
| Y1437 | *MATa MET-HA3-CDC20 CYK3-HA6* | This study |
| Y1438 | *MATa MET-HA3-CDC20 CYK3-HA6 cdc55Δ* | This study |
| Y1454 | *MATa MET-HA3-CDC20 MYO1-TOMATOE SPC42-GFP INN1-GFP* | This study |
| Y1491 | *MATa MET-HA3-CDC20 MYO1-FLAG IQG1-HA6 HOF1-MYC9* | This study |
| Y1497 | *MATα MET-HA3-CDC20 MYO1-FLAG IQG1-HA6 cdc55Δ* | This study |
| Y1512 | *MATa MET-HA3-CDC20 MYO1-TOMATOE SPC42-GFP cdc55Δ* | This study |
| Y1516 | *MATa MET-HA$_3$-CDC20 CHS2-GFP SPC42-GFP* | This study |
| Y1565 | *MATa MET-HA3-CDC20 CYK3-HA6 PK3-CDC55* | This study |
| Y1566 | *MATa MET-HA3-CDC20 INN1-HA6 PK3-CDC55* | This study |
| Y1567 | *MATa MET-HA3-CDC20 CHS2-HA6 PK3-CDC55* | This study |
| Y1572 | *MATa MET-HA3-CDC20 MYO1-TOMATOE SPC42-GFP yE-GFP-IQG1* | This study |
| Y1574 | *MATa MET-HA3-CDC20 MYO1-TOMATOE SPC42-GFP CYK3-GFP* | This study |
| Y1575 | *MATa MET-HA3-CDC20 MYO1-TOMATOE CHS2-GFP cdc55Δ* | This study |
| Y1576 | *MATα MET-HA3-CDC20 MYO1-TOMATOE SPC42-GFP CHS2-GFP* | This study |
| Y1578 | *MATa MET-HA3-CDC20 MYO1-TOMATOE HOF1-GFP cdc55Δ* | This study |
| Y1588 | *MATa MET-HA3-CDC20 SHS1-HA6* | This study |
| Y1589 | *MATa MET-HA3-CDC20 SHS1-HA6 cdc55Δ* | This study |
| Y1596 | *MATα MET-HA3-CDC20 MYO1-TOMATOE chs3Δ cdc55Δ* | This study |
| Y1604 | *MATa MET-HA3-CDC20 MYO1-TOMATOE SPC42-GFP CYK3-GFP cdc55Δ* | This study |
| Y1605 | *MATα MET-HA3-CDC20 MYO1-TOMATOE chs3Δ* | This study |

| | | |
|---|---|---|
| Y1606 | *MATa MET-HA3-CDC20 MYO1-TOMATOE SPC42-GFP yE-GFP-IQG1 cdc55Δ* | This study |
| Y1608 | *MATa MET-HA3-CDC20 MYO1-TOMATOE SPC42-GFP INN1-GFP cdc55Δ* | This study |
| Y1639 | *MATa MET-HA3-CDC20 CYK3-HA6 INN1-Myc9* | This study |
| Y1640 | *MATa MET-HA3-CDC20 CYK3-HA6 INN1-Myc9 cdc55Δ* | This study |
| Y1652 | *MATa MET-HA3-CDC20 MYO1-TOMATOE cdc55Δ URA3::HA3-CDC55* | This laboratory |
| Y1653 | *MATa MET-HA3-CDC20 MYO1-TOMATOE cdc55Δ URA3::HA3-CDC55-T174E_S301D* | This laboratory |
| Y1708 | *MATa MET-HA3-CDC20 MYO1-TOMATOE 3GFP-RAS2 cdc55Δ* | This study |
| Y1717 | *MATa MET-HA3-CDC20 MYO1-TOMATOE 3GFP-RAS2* | This study |
| Y1725 | *MATa MET-HA3-CDC20 MYO1-TOMATOE CDC15-eGFP cdc55Δ cdc28-Y19F* | This study |
| Y1728 | *MATa ADH1-AtTIR1-MYC9 hof1-aid* | Alberto Sánchez-Díaz |
| Y1730 | *MATa GAL1-UBR1 ADH1-AtTIR1-MYC9 td-cyk3-aid* | Alberto Sánchez-Díaz |
| Y1747 | *MATa GAL1-UBR1 ADH1-AtTIR1-MYC9 td-cyk3-aid cdc55Δ* | This study |
| Y1749 | *MATa ADH1-AtTIR1-MYC9 hof1-aid cdc55Δ* | This study |
| Y1761 | *MATa MYO1-TOMATOE CDC15-eGFP cdc28-Y19F* | This study |
| Y1788 | *MATα MET-HA3-CDC20 MYO1-TOMATOE SPC42-GFP pGPD1-OsTIR1-MYC9 cdc55-aid* | This study |
| Y2231 | *MATa MET-HA3-CDC20 CDC5-PK3 CDC14-HA6* | This laboratory |
| Y1852 | *MATa MET-HA3-CDC20 MYO1-TOMATOE GAL-CHS2-YFP cdc55Δ* | This study |
| Y1853 | *MATa MET-HA3-CDC20 MYO1-TOMATOE SPC42-GFP GAL-CHS2-YFP* | This study |
| Y1855 | *MATa MET-HA3-CDC20 MYO1-TOMATOE SPC42-GFP GAL-chs2-S14E-S60E-S69E-S86E-S100E-S133E-YFP* | This study |
| Y1857 | *MATa MET-HA3-CDC20 MYO1-TOMATOE SPC42-GFP GAL-chs2-S14A-S60A-S69A-S86A-S100A-S133A-YFP cdc55Δ* | This study |